A Global Temporal Genetic Program for Neural Circuit Formation

Saumya Jain[1,4], Ying Lin[1,2,4], Yerbol Kurmangaliyev[3], Parmis Mirshahidi[1], Brianna Parrington[1], and S. Lawrence Zipursky[1,3,*]

[1]Department of Biological Chemistry, University of California, Los Angeles, USA. [2]Molecular Biology Institute, University of California, Los Angeles, USA. [3]Howard Hughes Medical Institute, David Geffen School of Medicine, University of California, Los Angeles, USA. [4]These authors contributed equally to this work. [*]e-mail: lzipursky@mednet.ucla.edu

Wiring a complex brain relies on cell-type and temporal-specific expression of genes encoding cell recognition molecules regulating circuit formation[1–3]. Though genetic programs driving cell-type specificity have been described[4–6], how precise temporal control is achieved remains unknown. Here, we describe a global program for the temporal regulation of cell-type-specific wiring genes in the *Drosophila* visual system. We show that the Ecdysone Receptor induces a synchronous cascade of transcription factors in neurons throughout the visual system in a highly stereotyped fashion. Single-cell RNA-seq analysis of neurons lacking transcription factors in the cascade revealed that targets are cell-type dependent and these are enriched for wiring genes. Knock-down of different transcription factors in this cascade led to defects in sequential steps in wiring. Taken together, this work identifies a synchronous, global program for temporal control of different sets of wiring genes in different neurons. We speculate that this global program coordinates development across cell types to choreograph specific steps in circuit assembly.

MAIN

Animal behavior is dependent upon the formation of neuronal circuits with high fidelity. Many cell-surface proteins, particularly of the Immunoglobulin (Ig), Leucine-Rich Repeat and Cadherin families, promote interactions between neurons during circuit assembly[1,7]. Several developmental strategies have evolved to meet the demands of cellular recognition specificity during circuit construction. These include the expression of combinations of different recognition molecules in different neurons, and reusing the same molecules to determine multiple, spatially and temporally separated neuron-neuron interactions[2,3,8]. Wiring specificity, thus, relies critically on genetic programs which regulate the cell-type and temporal specificity of genes encoding recognition molecules. Many programs that define cell-type specificity have been described[4–6]. Here we set out to assess how temporal specificity is determined.

Dynamic expression of wiring genes

To identify genetic programs regulating the temporal control of wiring genes, we profiled the transcriptomes of post-mitotic lamina neurons (L1-L5) in the *Drosophila* optic lobe (analogous to bipolar cells in the mammalian retina[8]), every 12h from 24hAPF (hours After Pupa Formation) to adults (Fig. 1a, b). These time points encompass all aspects of circuit formation for lamina neurons once their growth cones have reached their target neuropil[9,10]. For transcriptional profiling, we modified a recently developed single-cell RNA-Seq-based approach that utilizes the natural genetic variation (i.e detected by single nucleotide polymorphisms (SNPs)) amongst different *Drosophila* wildtype lines (DGRP[11]) to determine gene expression in many different samples and different time points in one experiment (Kurmangaliyev *et al*. revision under review, Fig. 1b, Extended data Fig. 1, Supplementary Table 1). This approach eliminates issues due to

batch effects that limit transcriptome analyses combining data from independent experiments. Using this approach, we acquired transcriptomic data for 8269 cells distributed between seven timepoints (24hAPF – Adult) (Fig. 1b, Extended data Fig. 1b, Supplementary Table 2). Using the SNPs within the transcripts encoded by the different DGRP strains, we assigned each cell to a specific time point. We integrated all cells and performed unsupervised clustering independent of global changes occurring over time yielding five clusters (see Methods). We used previously identified lamina neuron-type specific genes to assign each cluster to a cell-type[12] (Extended data Fig. 1c). For all subsequent analyses, we used normalized gene expression values prior to integration. The expression patterns were similar to expression data from bulk RNA-seq (this study, Supplementary Table 3) and from a large single cell sequencing study of visual system neurons from our laboratory (Kurmangaliyev *et al.* revision under review) (Extended data Fig. 2).

Application of k-means clustering to group genes based on their expression dynamics revealed several groups that showed dynamic patterns of expression (e.g. gene groups 5, 7, 9 and 10 in Fig. 1c; also see Extended data Fig. 3 and Supplementary Table 4). Dynamically expressed genes (especially early-peaking gene groups) were enriched (over expected by chance) for genes encoding Immunoglobulin Superfamily (IgSF) proteins, as well as GO terms related to wiring (Fig. 1c, Extended data Fig. 3, Supplementary Table 5). Genes encoding IgSF proteins expressed in a dynamic temporal fashion (see Methods), were also expressed in a cell-type-dependent manner (Extended data Fig. 4a). Thus, as previously described[13,14], wiring genes are expressed in a cell-type and temporally dynamic fashion during circuit assembly.

Synchronous expression of the EcR Cascade

To identify transcription factors (TFs) that drive gene expression in a dynamic fashion, we looked at TFs that were differentially expressed between pairs of consecutive time points for each neuron-type across development (Extended data Fig. 4b, see Methods). Interestingly, for each neuron-type, dynamically expressed TFs were enriched for the *Nuclear Receptor Transcription Factor Pathway* (Reactome Pathway Enrichment Analysis[15], p-value < 10^{-5}, Extended data Fig. 4c). These TFs, including the **Ec**dysone **R**eceptor (EcR) and others regulated by Ecdysone[16,17], exhibit synchronous patterns of expression in lamina neurons over development (red lines in Fig. 2a, Extended data Fig. 5a, b). In addition, EcR also undergoes a temporal-specific isoform switch due to the use of an alternative transcription start site, from predominantly EcR-B1 to EcR-A in these neurons (Fig. 2a, Extended data Fig. 5), as determined by staining with isoform-specific antibodies and bulk RNA sequencing. This temporal switch in isoform expression has been reported previously for other neurons in the central nervous system[18].

Immunostaining for EcR-B1, EcR-A, Hr3 and Ftz-f1 (Extended data Fig. 5a), and our analysis of the whole optic lobe transcriptome (Kurmangaliyev *et al.* revision under review) revealed that this transcriptional cascade has near-synchronous dynamics in all optic lobe neurons throughout development (Fig. 2a). The timing and order of expression of these TFs correlates with a mid-pupal pulse of Ecdysone[16,17,19–21] (Fig. 2a). A role for this transcriptional cascade in various developmental contexts, including neuronal remodeling of specific neuron-types during metamorphosis has been studied in detail[22,23]. The coordinate and visual-system-wide expression of these transcription factors during pupal development raised the intriguing possibility that this cascade acts as a temporal regulator of circuit formation more broadly.

Temporal control of cell-type specific wiring genes

We next sought to address whether the EcR cascade drives the temporal expression of genes in lamina neurons. Analysis of putative cis-regulatory regions[24] for dynamically expressed genes in lamina neurons showed a significant enrichment for binding sites for TFs in the EcR cascade (Supplementary Table 6, see Methods), consistent with their direct role in driving these patterns of gene expression. Additionally, ATAC-Seq[25] at 40hAPF, 60hAPF and 72hAPF in L1 neurons (see Methods and Extended data Fig. 6, Supplementary Table 7) identified an enrichment for predicted binding sites for TFs in this cascade (e.g. EcR, Hr3, Hr4 and Ftz-f1) in regions with dynamic patterns of accessibility[24] (Extended data Fig. 6d, Supplementary Table 6). This is consistent with these TFs controlling chromatin structure, transcription of specific genes or both[26].

To identify genes regulated by the EcR cascade, we targeted expression of a dominant negative allele of EcR (EcR^{DN}, EcR-B1 W650A[27]), EcR RNAi and Hr3 RNAi to lamina neurons. Transcriptional profiling was performed using a single-cell RNA-Seq-based assay (Fig. 2b) to compare transcriptomes of wildtype and mutant lamina neurons at four timepoints (24hAPF, 48hAPF, 72hAPF and Adult) in a pooled fashion using the DGRP strategy (Supplementary Table 1). By comparing the transcriptomes of 3606 wildtype and 1503 EcR^{DN}-expressing lamina neurons, we identified 921 differentially expressed genes (fold change ≥ 2, p-value ≤ 0.05), out of a total of 3200 genes expressed in lamina neurons across development. These were distributed between the five lamina neuron-types and four time-points (Extended data Fig. 7, Supplementary Table. 8). Importantly, EcR^{DN}-expressing lamina neurons continued to express their cell-type specific TFs, suggesting no changes in cell-fate (Extended date Fig. 7b). In contrast to L1 and L3-L5, EcR^{DN} had modest effects on gene expression in L2. This is consistent with lower EcR^{DN} expression in L2 neurons at 48hAPF using this GAL4 driver line (Extended data Fig. 7e). Analysis

of the 921 differentially expressed transcripts led to four conclusions. First, EcR-dependent genes are enriched for those showing dynamic expression in wildtype cells (Extended data Fig. 7f, 11). Second, a large set of genes dependent upon this cascade is expressed in a cell-type-dependent fashion in wildtype lamina neurons (Fig. 2c, Extended data Fig. 8). Third. the cell-type dependent genomic targets of this cascade were highly enriched for IgSF genes (Hypergeometric test, p-value = 1.25×10^{-18}, see Methods) as well as GO terms associated with wiring (Fig. 2d, e, Supplementary Table 9). And finally, it was not uncommon for EcR^{DN} to have different effects on the same gene in different neuron types. This may reflect different levels of expression of EcR^{DN}. In some cases, however, opposite effects in different lamina neurons were observed (Fig. 2d).

Three lines of evidence indicated that genes affected by the expression of EcR^{DN} were largely bona fide targets of this transcriptional cascade. First, most genes affected by EcR^{DN} were affected in a similar way by EcR RNAi, although the change was typically less pronounced (Extended data Fig. 9, 12a; Supplementary Table 10). Second, changes in gene expression in Hr3 RNAi and EcR^{DN} were similar, especially at later time points, as expected from their genetic relationship (Fig. 2a; Extended data Fig. 10, 12b; Supplementary Table 11). And third, expression of several putative EcR-dependent genes in brains cultured *ex vivo*[28] depended on the inclusion of Ecdysone in the medium (see Methods, Extended data Fig. 13, 16b). Thus, EcR, either directly or indirectly, controls the temporal expression of wiring genes in a cell-type-specific manner.

The cell-type-specific, temporal control of wiring genes by the EcR cascade suggests that it plays a role in circuit formation. Consistent with this notion, we observed a disorganization of lamina neuron arbors in the medulla neuropil upon pan-lamina expression of EcR^{DN}, which was largely rescued by overexpression of wildtype EcR-B1 (Extended data Fig. 14a). A disorganized neuropil was also seen upon targeted expression of EcR RNAi. Disruption of the axon terminal

morphology of T4/T5 neurons in the lobula plate neuropil, a more central visual system structure, was also seen upon targeted expression of EcR^{DN} to these neurons (Extended data Fig. 14b). Together these data support the idea that the EcR transcriptional cascade regulates genetic programs governing the appropriate expression of cell surface and secreted proteins required for proper wiring of the visual system.

EcR regulates the L3-specific expression of Netrin

We next sought to assess whether loss of EcR function gave rise to similar phenotypes seen for loss-of-function mutations in cell surface or secreted proteins regulating wiring in L1-L5. Loss of EcR activity resulted in phenotypes similar to *Netrin* mutants in L3[29,30] (Fig. 3a-d) and mutations in *DIP-β,* encoding an IgSF protein, in L4[31] (Extended data Fig. 15). Here we focus on the relationship between *EcR* and *Netrin*.

Netrin protein is required in L3 axon terminals in the M3 layer to promote adhesion of photoreceptor R8 growth cones to processes in the same layer. In *Netrin* mutants, R8 terminals extend into the developing M3 layer, but are unable to stably adhere to it and retract to the surface of the medulla[30]. At least one other, yet to be identified, signal is necessary for R8 to recognize the M3 layer[30]. From sequencing of mutants and anti-Netrin antibody staining, EcR activity is required for Netrin expression in L3 (Fig. 3a, b, Extended data Fig. 16b). Targeting expression of EcR^{DN} in L3 leads to an R8 mis-targeting phenotype. Here most R8 terminals extend beyond the M3 layer and some remain at the surface of the medulla. The EcR^{DN} phenotype is partially rescued by overexpression of Netrin in developing EcR-mutant L3 neurons (Fig. 3c). Differences between the *Netrin* mutant and EcR^{DN} phenotypes are consistent with the notion that EcR regulates one or more signals in L3, in addition to Netrin, necessary for R8 targeting[30] (Fig. 3d).

As EcR is expressed in the same way in all lamina neurons, how is the cell-type specificity of wiring genes determined? Interestingly, genes specifically expressed in L3, including *Netrin*, are enriched for targets of the L3-specific TF Erm identified in a previous study[12] (Hypergeometric test, p-value = 2.7 X 10^{-18}; Fig. 3e; Extended data Fig. 17). Erm is expressed selectively in L3 early in lamina development and remains expressed into the adult[12,32] (Extended data Fig. 1c). Thus, here the EcR pathway confers temporal specificity to a continuously expressed cell-type-specific TF to ensure the precise spatial and temporal expression of wiring genes.

Stepwise assembly of L5 connectivity

We next sought to assess whether the EcR cascade regulates sequential steps in wiring. For this we turned to L5. L5 axon morphology in the medulla forms in a stepwise manner[33] (Fig. 4b). L5 targets to M5 and then arborizes in M1 and M2 (M1/2) (Fig. 1a, 4b). Arborization occurs in two steps: 1) initial branching in M1 (between 48hAPF and 60hAPF) and, 2) growth from M1 to M2 (between 75hAPF and 90hAPF) (Fig. 4b). EcR^{DN} or EcR RNAi expression blocks step 1, while Hr3 and ftz-f1 RNAi each blocks step 2 (Fig. 4a, b). These findings are consistent with the notion that EcR regulates the expression of genes that promote extension of dendrites into M1 and that Hr3 and Ftz-f1 execute a subsequent developmental step, some 24 hours later (Fig. 4b). Hr3 directly regulates *ftz-f1* expression[17] (see Fig. 2a, Extended data Fig. 10d). Thus, Ftz-f1 may act alone or in combination with Hr3, to regulate the expression of a set of genes necessary to control targeting of dendrites to M2. As L5 makes synaptic connections with different partners in M1 and M2[34], EcR may control cell surface proteins regulating synaptic specificity in M1, whereas synaptic specificity in M2 may be controlled by cell recognition proteins regulated by Hr3, Ftz-f1, or both.

168 The phenotypes resulting from Hr4 RNAi are qualitatively different from knocking down
169 levels of EcR, Hr3 and Ftz-f1. Loss of Hr4 results in promoting extension of L5 branches beyond
170 M2 to M5 (Fig. 4a). Hr4 may regulate a stop signal, preventing extension beyond M2 to deeper
171 layers. Alternatively, as Hr4 is expressed at a much earlier step in development (see Fig. 2a), it
172 may repress a growth pathway acting in the initial extension into M1. As knock down experiments
173 of EcR pathway components led to marked changes in the expression of genes encoding different
174 cell surface and secreted proteins implicated in wiring (Fig. 4c, Supplementary Table 12), these or
175 discrete combinations of them, may function at different steps or in specific spatial domains of L5
176 axons to establish specific patterns of synaptic connections.

177 **Discussion**

178 Wiring the brain requires precise cell-type and temporally restricted expression of genes
179 encoding cell surface proteins[2,3,12,13,35]. Our studies uncovered a strategy that plays a widespread,
180 yet specific role, in regulating this process. We describe a genetic program expressed in most, if
181 not all, visual system neurons that controls the precise temporal patterns of expression of wiring
182 genes (Fig. 4d). These have cell-type specific outputs which reflect the integration of a shared
183 temporal program with diverse pathways controlling the development of different cell types. We
184 show that this temporal program regulates discrete steps in wiring specificity.

185 The timing of expression of wiring genes results from the activation of a transcriptional
186 cascade by the steroid hormone Ecdysone, comprising multiple transcription factors (such as EcR,
187 Hr3 and Ftz-f1) including members of the nuclear receptor family. These produce sequential waves
188 of gene expression[16] (Fig. 2, 4d) which regulate different steps in wiring in different neurons. The
189 control of a cell-type-specific set of wiring genes is made possible, at least in part, by a

combinatorial mechanism in which many members of this transcriptional cascade work with different cell-type-specific TFs to produce different outputs[36–38]. Mechanisms that establish cellular transcriptional landscapes early in development have been identified[39–41], including cell-type-specific TFs (e.g. Erm). These are expressed in postmitotic neurons and determine multiple cell-type-dependent features, including transcription of genes required for circuit formation[4,42,43]. By extrapolation of the dual control of Netrin by Erm and EcR in L3, we speculate that it is the coordinate activities of these two classes of TFs that regulates developmental programs specifying connectivity.

Dynamic expression of wiring genes, including cell-recognition molecules, poses an additional challenge for gene expression control. How are the transcriptomes of diverse neuron-types coordinated to ensure proper wiring? A global temporal signal, such as Ecdysone, is a possible mechanism to coordinate the development of multiple neuron types. For instance, the Ecdysone-dependent timing of Netrin expression in L3 growth cones matches the arrival of R8 growth cones in M3 (Fig. 3d; Extended data Fig. 16a). Further experiments will be necessary to determine whether Ecdysone not only regulates the timing of developmental steps, but also ensures that these are coordinated between different neuron-types in the complex choreography leading to circuit assembly.

Our studies rest on decades of genetic and biochemical experiments establishing the Ecdysone-pathway as a temporal regulator of major developmental transitions, including larval molts and metamorphosis, as well as controlling sequential divisions of postembryonic neuroblasts and neuronal re-modelling[16,23,37,38,44]. Here we show that this program has been co-opted for the temporal regulation of differentiation, and the coordinate development of different neuron types leading to the complex circuitry of the fly visual system. The ability of the EcR cascade to function

as a flexible temporal regulatory module used in multiple developmental contexts may be similar to modules regulating spatial patterning (e.g. Hox genes and BMP/Wnt/Hh pathways[45–47]) which act in context-dependent ways to generate different morphological outcomes. These findings raise the intriguing possibility that similar timing mechanisms may also regulate the sequence of events regulating wiring in other systems[48] including the maturational sequence in the assembly of neural circuits in the mammalian brain[49].

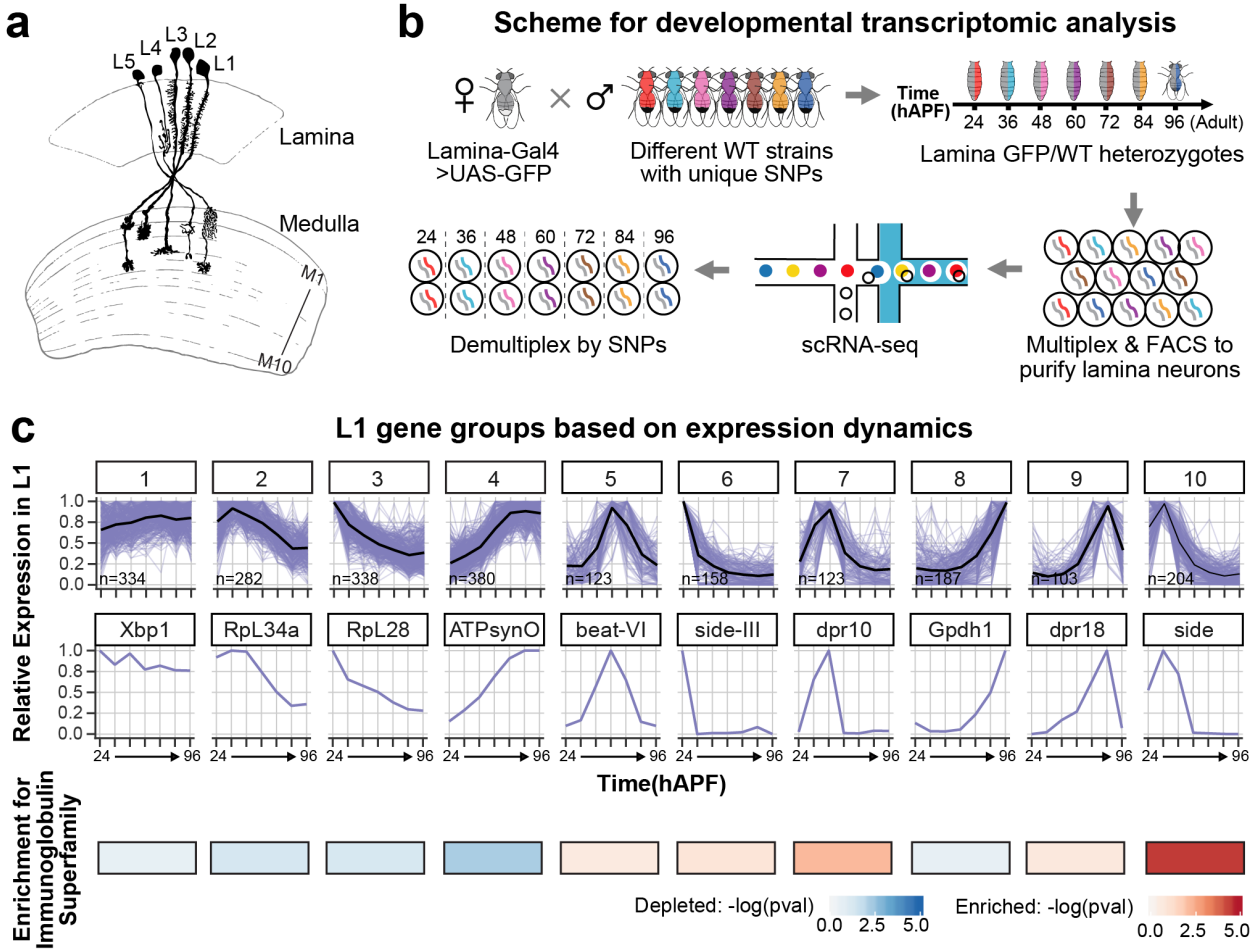

Fig. 1 | A developmental transcriptome reveals dynamic expression of wiring genes. a, Lamina neurons (L1-L5) in the *Drosophila* visual system project axons into the medulla. **b,** Scheme for single-cell RNA-Seq of lamina neurons (see Methods) using wildtype strains (DGRP) with unique SNPs as bar codes. Each time point includes lamina neurons from three animals, each heterozygous for a different SNP bar code. In total 21 different DGRP lines were used in this experiment. Thus, the transcripts of cells from each animal and their developmental stage (hours after pupal formation (hAPF)) were identified by unique SNPs. **c,** Gene groups generated via k-means clustering using expression dynamics in L1 neurons (see Methods; for other lamina neurons see Extended data Fig. 3). Relative expression over development for each gene in the group is shown as a line plot (purple lines), with the mean shown as a black line. n, number of genes in the

group. A gene from each group is shown (e.g. Xbp1). Heat map depicts enrichment ($-\log_{10}$ p-values) of Immunoglobulin Superfamily genes over that expected by chance (see Methods).

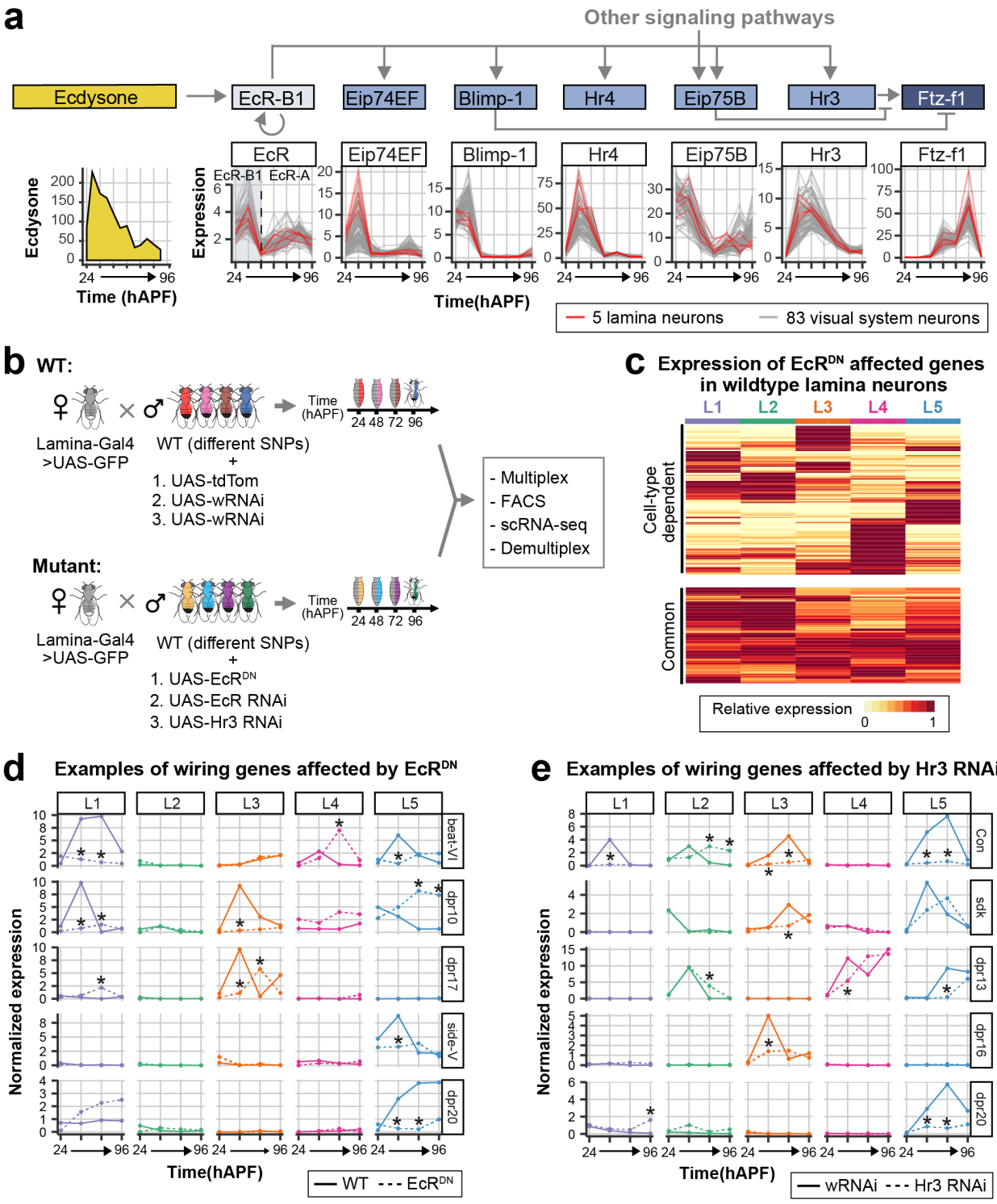

231 **Fig. 2 | Wiring genes in different cell-types are controlled by an Ecdysone-induced**

232 **transcriptional cascade. a,** Schematic of the genetic interactions between transcription factors of

the Ecdysone-induced transcriptional cascade. Only a subset of the known interactions is shown. In the plots, red lines show normalized expression of these transcription factors in lamina neurons and grey lines show expression dynamics in 83 other neuron-types (data from Kurmangaliyev *et al.* revision under review) (bottom). Isoform change from EcR-B1 to EcR-A during development is shown. Concentration of circulating Ecdysone over development is shown on the left (adapted from Pak and Gilbert[21]) **b,** Scheme for scRNA-Seq-based analysis of genes affected by perturbation of EcR or Hr3 activity in lamina neurons. Mutant and control brains for each perturbation were analyzed together in three separate experiments. UAS-tdTom and UAS-wRNAi were use as controls for EcR^{DN} and EcR (and Hr3) RNAi, respectively. **c,** Heat map showing relative expression in wildtype cells of genes affected by EcR^{DN} at 48hAPF. Targets of EcR are divided into two categories: Cell-type dependent, in any pairwise comparison fold difference ≥ 2, p-value ≤ 0.05, 303 genes; Common targets, all remaining EcR targets, 208 genes. **d,** Expression of some wiring genes affected by EcR^{DN}. Solid line, expression in wildtype cells; Dashed line, expression in EcR^{DN} cells. **e,** Expression of some wiring genes altered by Hr3 RNAi. Solid line, expression in wildtype cells; Dashed line, expression in Hr3 RNAi cells; *, difference in expression between wildtype and perturbation $\geq$ 2-fold, p-value ≤ 0.05.

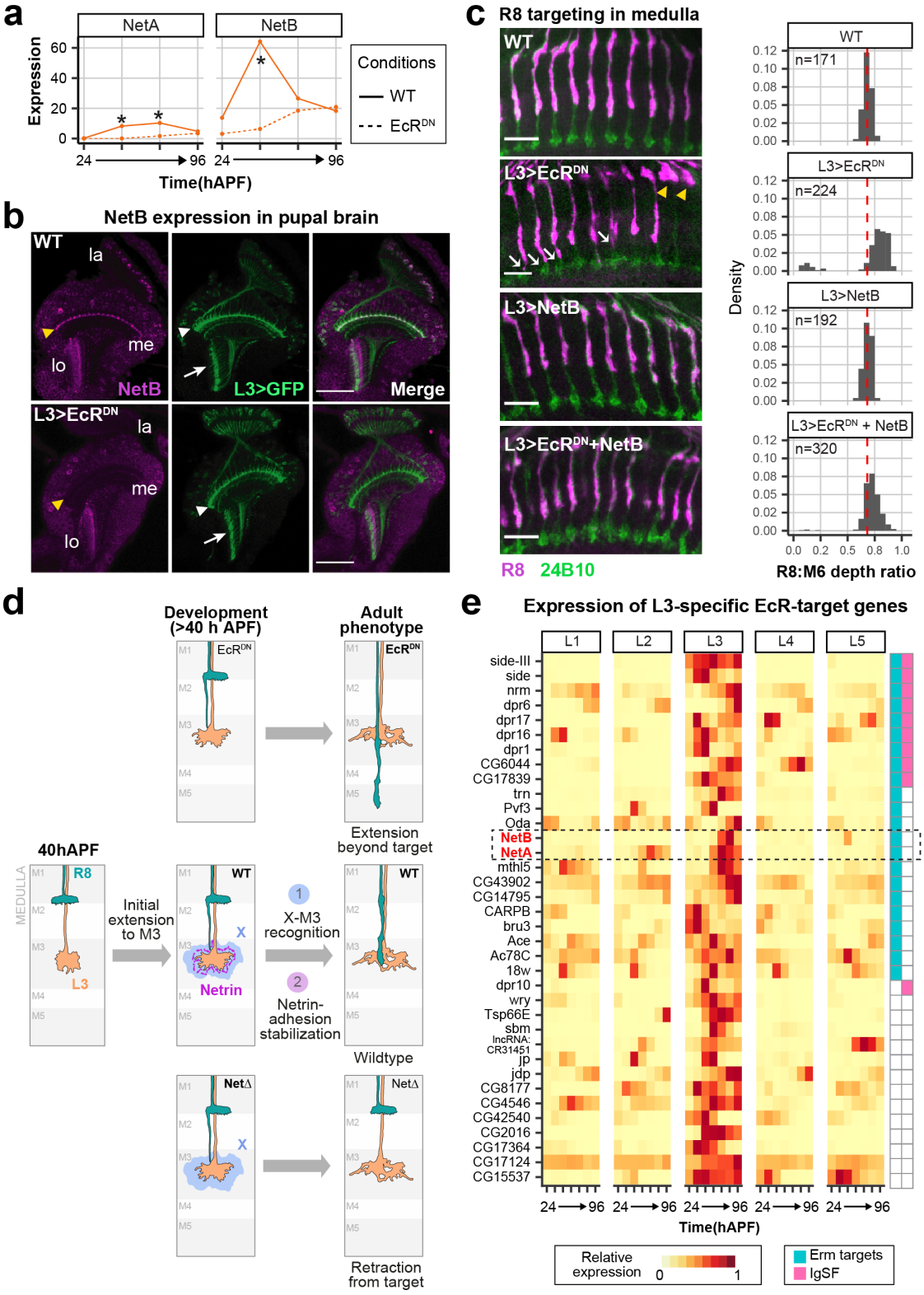

249 **Fig. 3 | EcR-dependent program in L3 neurons controls R8 targeting. a,** Normalized

250 expression of NetrinA (NetA) and NetrinB (NetB) over development in WT (solid lines) and

EcR^{DN} (dashed lines) expressing L3 neurons. *, difference in expression between wildtype and EcR^{DN} ≥ 2-fold, p-value < 0.05. **b,** Anti-NetB staining (magenta) at 48hAPF ± EcR^{DN} expression in L3 neurons (green). Netrin expression in M3 is lost in response to EcR^{DN}. Note, as an internal control, that NetB expression in the lobula (lo) is not affected. la, lamina; me, medulla; yellow arrowhead, M3 layer; white arrowheads, L3 growth cones (some other cell types with axons in the lobula are also labeled (white arrows)). Scale bar, 50μm. **c,** Morphology of R8 axons (magenta) with wildtype L3 neurons (top). Other panels from top to bottom show L3s expressing EcR^{DN}, NetB and both EcR^{DN} and NetB. Left panels: R8 axons extending beyond M3 (white arrows); R8 axons terminals above the medulla neuropil (yellow arrowheads). Scale bar, 10μm. Right column, distribution of R8 axon depths represented as ratio of depth of R8 to M6 (medulla layer 6 indicated in green in the left panels). Red line, median of the distribution in wildtype. Distribution with WT and EcR^{DN} expressing L3 is significantly different (Kolmogorov-Smirnov test, p-value < 10^{-15}, see Extended data Fig. **16c** for other comparisons). n, number of neurons observed (6-10 animals for all conditions). **d,** Model for control of R8 targeting by L3. EcR controls expression of Netrin and one or more other molecules (X) in L3. Netrin is required for adhesion of R8 growth cones to processes in M3 and X is required for recognition of M3 by R8 growth cones to terminate extension[30]. **e,** Heat map showing relative expression of L3-specific targets of EcR (see Methods). Aqua, targets of transcription factor Erm identified in Peng *et al.*[32]; Magenta, Immunoglobulin Superfamily genes; Dashed lines, NetA and NetB.

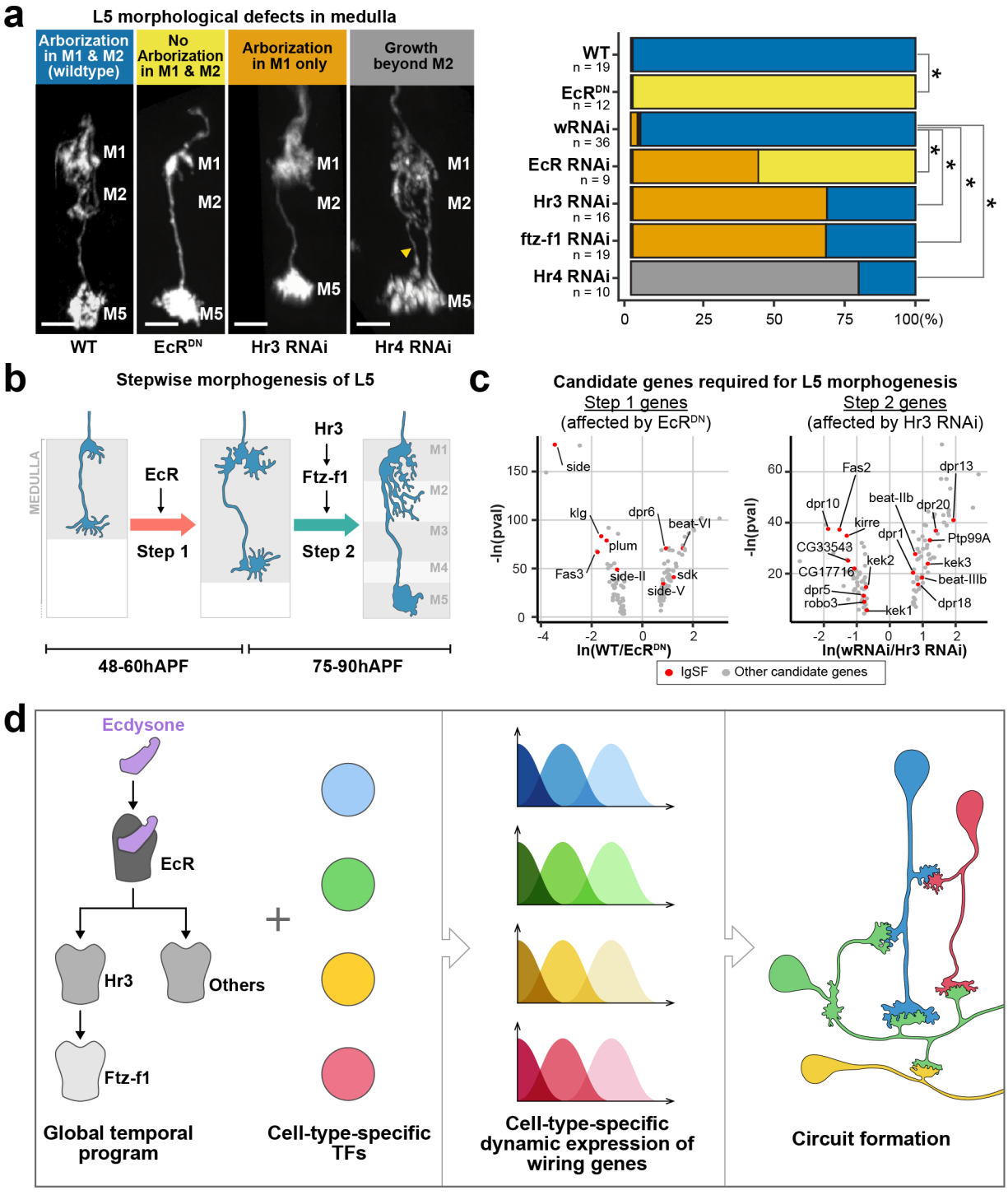

270 **Fig. 4 | The EcR cascade controls the stepwise arborization of L5 axons. a,** L5 axonal

271 arborization defects (left) and their distributions in wildtype L5's, or under pan-lamina expression

272 of EcR^{DN}, EcR RNAi, Hr3 RNAi, Hr4 RNAi or ftz-f1 RNAi (right). *, Fisher's exact test p-value

< 0.01. n, number of neurons observed (4 -13 animals for all conditions). In wildtype only the axon extends to M5; L5 neurons in Hr4 RNAi animals extend an additional process to M5. Scale bars, 5μm. **b,** Schematic of the stepwise morphogenesis of L5 in the medulla[33] showing the expected roles for EcR, Hr3 and Ftz-f1 based on data in panel a) and previous biochemical and gene expression studies (see Fig. 2a). The role of Hr4 in this process is unclear (see text). **c,** Volcano plots showing candidate genes involved in step1 (Left, 131 genes, significantly affected in EcR^{DN} at 48hAPF and not affected in Hr3 RNAi at any timepoint) and step2 (Right, 124 genes, significantly affected in Hr3 RNAi at 72hAPF, regardless of effect of EcR^{DN}) of L5 arborization. Immunoglobulin Superfamily genes are highlighted. **d,** Model: Control of wiring genes through a global temporal program acting in combination with cell-type-specific transcription factors (see Discussion). Other temporal regulators may also contribute to wiring.

References

1. Südhof, T. C. Towards an Understanding of Synapse Formation. *Neuron* **100**, 276--293 (2018).

2. Hassan, B. A. & Hiesinger, P. R. Beyond Molecular Codes: Simple Rules to Wire Complex Brains. *Cell* **163**, 285--291 (2015).

3. Yogev, S. & Shen, K. Cellular and Molecular Mechanisms of Synaptic Specificity. *Annu Rev Cell Dev Bi* **30**, 417--437 (2014).

4. Hobert, O. Chapter Twenty-Five - Terminal Selectors of Neuronal Identity. in *Current Topics in Developmental Biology* (ed. Wassarman, P. M.) vol. 116 455--475 (Academic Press, 2016).

5. Hong, W. & Luo, L. Genetic Control of Wiring Specificity in the Fly Olfactory System. *Genetics* **196**, 17--29 (2014).

6. Dasen, J. S. & Jessell, T. M. Chapter Six Hox Networks and the Origins of Motor Neuron Diversity. in *Current Topics in Developmental Biology* vol. 88 169--200 (Academic Press, 2009).

7. Zipursky, S. L. & Sanes, J. R. Chemoaffinity Revisited: Dscams, Protocadherins, and Neural Circuit Assembly. *Cell* **143**, 343--353 (2010).

8. Sanes, J. R. & Zipursky, S. L. Design Principles of Insect and Vertebrate Visual Systems. *Neuron* **66**, 15--36 (2010).

9. Pecot, M. Y. *et al.* Sequential Axon-Derived Signals Couple Target Survival and Layer Specificity in the Drosophila Visual System. *Neuron* **82**, 320--333 (2014).

10. Chen, Y. *et al.* Cell-type-Specific Labeling of Synapses In Vivo through Synaptic Tagging with Recombination. *Neuron* **81**, 280--293 (2014).

306 11. Mackay, T. F. C. *et al.* The extitDrosophila melanogaster Genetic Reference Panel. *Nature*
307 **482**, 173--178 (2012).
308 12. Tan, L. *et al.* Ig Superfamily Ligand and Receptor Pairs Expressed in Synaptic Partners in
309 Drosophila. *Cell* **163**, 1756--1769 (2015).
310 13. Li, H. *et al.* Classifying Drosophila Olfactory Projection Neuron Subtypes by Single-Cell
311 RNA Sequencing. *Cell* **171**, 1206--1220.e22 (2017).
312 14. Favuzzi, E. *et al.* Distinct molecular programs regulate synapse specificity in cortical
313 inhibitory circuits. *Sci New York N Y* **363**, 413--417 (2019).
314 15. Jassal, B. *et al.* The reactome pathway knowledgebase. *Nucleic Acids Res* **48**, D498--D503
315 (2020).
316 16. Riddiford, L. M., Cherbas, P. & Truman, J. W. Ecdysone receptors and their biological
317 actions. *Vitamins Hormones* **60**, 1--73 (2000).
318 17. White, K. P., Hurban, P., Watanabe, T. & Hogness, D. S. Coordination of Drosophila
319 metamorphosis by two ecdysone-induced nuclear receptors. *Sci New York N Y* **276**, 114--117
320 (1997).
321 18. Truman, J. W., Talbot, W. S., Fahrbach, S. E. & Hogness, D. S. Ecdysone receptor
322 expression in the CNS correlates with stage-specific responses to ecdysteroids during Drosophila
323 and Manduca development. *Dev Camb Engl* **120**, 219--234 (1994).
324 19. Agawa, Y. *et al.* Drosophila Blimp-1 Is a Transient Transcriptional Repressor That Controls
325 Timing of the Ecdysone-Induced Developmental Pathway. *Mol Cell Biol* **27**, 8739--8747 (2007).
326 20. Rabinovich, D., Yaniv, S. P., Alyagor, I. & Schuldiner, O. Nitric Oxide as a Switching
327 Mechanism between Axon Degeneration and Regrowth during Developmental Remodeling. *Cell*
328 **164**, 170--182 (2016).

21. Pak, M. D. & Gilbert, L. I. A Developmental Analysis of Ecdysteroids During the Metamorphosis of extitDrosophila Melanogaster. *J Liq Chromatogr* **10**, 2591--2611 (1987).

22. Boulanger, A. & Dura, J.-M. Nuclear receptors and Drosophila neuronal remodeling. *Biochimica Et Biophysica Acta Bba - Gene Regul Mech* **1849**, 187--195 (2015).

23. Alyagor, I. *et al.* Combining Developmental and Perturbation-Seq Uncovers Transcriptional Modules Orchestrating Neuronal Remodeling. *Dev Cell* **47**, 38--52.e6 (2018).

24. Imrichová, H., Hulselmans, G., Atak, Z. K., Potier, D. & Aerts, S. i-cisTarget 2015 update: generalized cis-regulatory enrichment analysis in human, mouse and fly. *Nucleic Acids Res* **43**, W57--W64 (2015).

25. Buenrostro, J. D., Wu, B., Chang, H. Y. & Greenleaf, W. J. ATAC-seq: A Method for Assaying Chromatin Accessibility Genome-Wide. *Curr Protoc Mol Biology Ed Frederick M Ausubel Et Al* **109**, 21.29.1--9 (2015).

26. Olivares, A. M., Moreno-Ramos, O. A. & Haider, N. B. Role of Nuclear Receptors in Central Nervous System Development and Associated Diseases. *J Exp Neurosci* **9**, 93--121 (2016).

27. Cherbas, L., Hu, X., Zhimulev, I., Belyaeva, E. & Cherbas, P. EcR isoforms in Drosophila: testing tissue-specific requirements by targeted blockade and rescue. *Development* **130**, 271--284 (2003).

28. Özel, M. N., Langen, M., Hassan, B. A. & Hiesinger, P. R. Filopodial dynamics and growth cone stabilization in Drosophila visual circuit development. *Elife* **4**, e10721 (2015).

29. Timofeev, K., Joly, W., Hadjieconomou, D. & Salecker, I. Localized Netrins Act as Positional Cues to Control Layer-Specific Targeting of Photoreceptor Axons in Drosophila. *Neuron* **75**, 80--93 (2012).

351 30. Akin, O. & Zipursky, S. L. Frazzled promotes growth cone attachment at the source of a
352 Netrin gradient in the Drosophila visual system. *Elife* **5**, e20762 (2016).
353 31. Xu, C. *et al.* Control of Synaptic Specificity by Establishing a Relative Preference for
354 Synaptic Partners. *Neuron* **103**, 865--877.e7 (2019).
355 32. Peng, J. *et al.* Drosophila Fezf coordinates laminar-specific connectivity through cell-
356 intrinsic and cell-extrinsic mechanisms. *Elife* **7**, (2018).
357 33. Nern, A., Zhu, Y. & Zipursky, S. L. Local N-Cadherin Interactions Mediate Distinct Steps in
358 the Targeting of Lamina Neurons. *Neuron* **58**, 34--41 (2008).
359 34. Takemura, S. *et al.* A visual motion detection circuit suggested by extitDrosophila
360 connectomics. *Nature* **500**, 175--181 (2013).
361 35. Kurmangaliyev, Y. Z., Yoo, J., LoCascio, S. A. & Zipursky, S. L. Modular transcriptional
362 programs separately define axon and dendrite connectivity. *Elife* **8**, e50822 (2019).
363 36. Barolo, S. & Posakony, J. W. Three habits of highly effective signaling pathways: principles
364 of transcriptional control by developmental cell signaling. *Gene Dev* **16**, 1167--1181 (2002).
365 37. Shlyueva, D. *et al.* Hormone-responsive enhancer-activity maps reveal predictive motifs,
366 indirect repression, and targeting of closed chromatin. *Mol Cell* **54**, 180--192 (2014).
367 38. Uyehara, C. M. & McKay, D. J. Direct and widespread role for the nuclear receptor EcR in
368 mediating the response to ecdysone in Drosophila. *Proc National Acad Sci* **116**, 9893--9902
369 (2019).
370 39. Erclik, T. *et al.* Integration of temporal and spatial patterning generates neural diversity.
371 *Nature* **541**, 365--370 (2017).
372 40. McDonald, J. A. *et al.* Dorsoventral patterning in the Drosophila central nervous system: the
373 vnd homeobox gene specifies ventral column identity. *Gene Dev* **12**, 3603--3612 (1998).

374 41. Cochella, L. & Hobert, O. Embryonic Priming of a miRNA Locus Predetermines Postmitotic
375 Neuronal Left/Right Asymmetry in C. elegans. *Cell* **151**, 1229--1242 (2012).
376 42. Kratsios, P. *et al.* Transcriptional Coordination of Synaptogenesis and Neurotransmitter
377 Signaling. *Curr Biol* **25**, 1282--1295 (2015).
378 43. Philbrook, A. *et al.* Neurexin directs partner-specific synaptic connectivity in C. elegans.
379 *Elife* **7**, e35692 (2018).
380 44. Syed, M. H., Mark, B. & Doe, C. Q. Steroid hormone induction of temporal gene expression
381 in Drosophila brain neuroblasts generates neuronal and glial diversity. *Elife* **6**, e26287 (2017).
382 45. Altmann, C. R. & Brivanlou, A. H. Neural patterning in the vertebrate embryo. *Int Rev Cytol*
383 **203**, 447–482 (2001).
384 46. Briscoe, J. & Small, S. Morphogen rules: design principles of gradient-mediated embryo
385 patterning. *Development* **142**, 3996–4009 (2015).
386 47. Gaunt, S. J. Hox cluster genes and collinearities throughout the tree of animal life. *Int J Dev*
387 *Biol* **62**, 673–683 (2018).
388 48. Lawson, H. *et al.* The Makorin lep-2 and the lncRNA lep-5 regulate lin-28 to schedule sexual
389 maturation of the C. elegans nervous system. *Elife* **8**, (2019).
390 49. McCarthy, M. M. Estradiol and the Developing Brain. *Physiol Rev* **88**, 91--124 (2008).

Methods

Fly husbandry and stocks

Maintenance and rearing of fly lines, as well as staging of pupae was done as described in Tan *et al.*[12] Fly lines used in this work are listed in Supplementary Table 1.

Multiplexed single cell transcriptomic analysis

For transcriptomic analysis of developing wildtype lamina neurons, w; UAS-H2A-GFP; 9B08-Gal4/Tm6B, tb females were crossed with males from different DGRP backgrounds (wildtype, see Supplementary Table 1 for list of DGRPs used). F1 prepupae were staged as in Kurmangaliyev *et al.*[35] Males were only included in the analysis if no significant differences in gene expression were found with female pupae of the same genotype and developmental time point. Pupae corresponding to different developmental stages (see Fig. 1b) were all dissected, dissociated and processed at the same time. Each developmental time point was represented by ≥ 2 DGRP heterozygotes, and only one animal/ DGRP heterozygote was dissected. Tissue dissociation, FACS and preparation of single-cell libraries using 10X Genomics Chromium (v3) were carried out similar to Kurmangaliyev *et al.*, except that H2A-GFP expression was used to enrich for lamina neurons (see Extended data Fig. 1a). All libraries were sequenced on a NextSeq500 platform (single-end 75bp).

For transcriptomic analysis involving UAS EcR^{DN} (BDSC #6872), males carrying a single DGRP autonomous chromosome – w; (UAS EcR^{DN} or UAS tdTom); DGRP/ Tm6b, tb were crossed with w; UAS-H2A-GFP; 9B08-Gal4/Tm6B females. For experiments involving UAS EcR RNAi (BDSC #9326) or UAS Hr3 RNAi (BDSC #27253), w; DGRP; (UAS wRNAi or UAS EcR RNAi or UAS Hr3 RNAi)/ Tm6B, tb males were crossed with UAS Dcr2; UAS H2A-GFP; 9B08

Gal4/ Tm6B, tb females (see Fig. 2b and Supplementary Table 1). UAS tdTom and UAS wRNAi were used as controls.

scRNA-seq data pre-processing

Raw fastq read files were processed using Cell Ranger (3.1.0) with default parameters. Seurat V3 was used for all preliminary analyses. FlyBase reference genome (release 6.29[50]) was used for alignment and annotation. Profiled single cells were identified as coming from a particular developmental time-point and genetic background based on the natural genomic variance within the different parent DGRP lines. This was done using the pipeline described in Kurmangalyev *et al.*, with the following modifications: the count of minor allele that equals to 2 among the analyzed DGRP strains were used as genomic variants to assign the profiled single cells to different DGRP parent lines. Only single cells with: 1) number of genes between 200 and 3000, 2) number of mitochondrial transcripts < 20% of all transcripts, and 3) assignment to a unique DGRP parent line; were used for all downstream analyses.

To identify different lamina neuron subtypes, all cells from a particular experiment were integrated as described in Seurat v3 workflow and then subjected to unsupervised clustering, thus disregarding global temporal gene expression changes (similar to Kurmangaliyev *et al.*). Previously identified lamina neuron subtype specific genes[12] were used to assign each cluster to a cell-type. Cells not assigned to a lamina neuron-type cluster were removed from subsequent analyses. Average expression for each gene for each cell-type at a particular timepoint and genetic background was calculated using normalized expression values prior to integration.

Bulk RNA-seq

Bulk RNA-Seq analysis of L1 neurons at 40hAPF, 60hAPF and 72hAPF was performed as in Tan *et al.*[12] At least 2 replicates were generated for each timepoint. A minimum of 2000 cells were sorted for each experiment. cDNA libraries were created using the SMART-Seq2 protocol[51], which were then sequenced together using the HiSeq4000 platform (paired-end 50bp).

Raw fastq reads files were mapped to FlyBase reference genome (release 6.29) using STaR (2.6.0) and only uniquely mapped reads were collected. Genes with counts per million (CPM) ≥ 4 in more than 2 samples were used for normalization with R package edgeR (3.26.8). Gene expression was quantified using RPKM units (Reads Per Kilobase of exon per Million reads mapped), calculated based on reads in the sum of exons using customized scripts. The correlation between biological replicates were calculated using Spearman correlation for top 500 genes with the highest variation across all samples.

Bulk ATAC- seq

At least 8000 L1 neurons were FACS purified at 40hAPF, 60hAPF and 72hAPF as described in Tan *et al.*[12] Biological duplicates were generated for each timepoint. ATAC-Seq libraries were generated as per the following protocol, which was modified from the one described in Buenrostro *et al.*[52]: 1) FACS purified cells were collected in 300ul 1X PBS and spun at 800xg for 8' at 4°C. 2) Cell pellet was then directly resuspended in 50µl of a tagmentation enzyme mix (25µl Nextera DNA library prep kit – Tagment DNA Buffer, 19µl Nuclease-free water, 5µl 1% IGEPAL CA630, 1µl Nextera DNA library prep kit - Tagment DNA Enzyme) and incubated at 37°C for 30' with constant agitation at 400rpm. 3) DNA was purified from the tagmentation mixes using the Qiagen minElute Reaction Cleanup Kit as per the manufacturer's protocol. 4) A 10µl

qPCR reaction was setup to determine the optimum number of amplification cycles (similar to Buenrostro *et al.*). 5) A larger PCR reaction (40µl) was then setup and PCR products in the 200-500bp range were gel purified. 6) Steps 4 and 5 were repeated, this time with barcoded primers (see Buenrostro *et al.*) to allow multiplexing of all libraries onto a single lane of HiSeq4000 (paired-end 50bp).

Raw fastq reads files were mapped to FlyBase reference genome (release 6.29) using Bowtie2 (2.2.9) and uniquely mapped genes were kept. All samples were pooled together prior to peak calling. Read start positions were shifted +4 or -5bp and used for peak calling using MACS2 (2.1.1) with parameters "-q 0.01 --nomodel --shift -100 --extsize 200". There were 26,122 peaks identified. Then bedtools multicov (2.27.1) was used to sum the total reads within each peak separately for each sample. Peaks with CPM ≥ 4 were used for counts normalization with edgeR. Correlations between biological replicates were calculated using Spearman correlation for the top 500 peak regions with the highest variation of peak levels across all samples. Distribution of the top 5000 peaks across different genomic features at 40hAPF, 60hAPF and 72hAPF was determined using the R package ChIPseeker (1.20.0). Differential peak analysis was performed using edgeR. Fold-change ≥ 2 and adjusted p-value ≤ 0.05 were chosen as the cutoffs to define peaks with differential accessibility between time points. Each ATAC peak was associated to the nearest gene based on proximity to the transcription start site using ChIPseeker. To compare change of ATAC-seq peak accessibility over time and change in expression of nearest gene, ln(fold change ATAC-seq peak read coverage) was plotted against ln(fold change expression of nearest gene) for each ATAC-Seq peak (Extended data Fig. 6). Bulk RNA-Seq data was used for this, as this transcriptome dataset had been generated for the same time points as for ATAC-Seq. This was

done separately for peaks differentially accessible between 40hAPF and 60hAPF (Extended data Fig. 6b (left)) and between 60hAPF and 72hAPF (Extended data Fig. 6b (right)).

Comparison of scRNA-Seq with other datasets

For comparison of lamina neuron transcriptomes generated here with lamina neuron transcriptomes generated in Kurmangaliyev *et al.*, 500 genes with the highest variance across all cell types and all timepoints were used to calculate Spearman correlation. Comparison of L1 transcriptome generated using scRNA-Seq and L1 transcriptome obtained from bulk RNA-Seq was done similarly.

k-means cluster analysis

Prior to clustering, all average gene expression from scRNA-seq transcriptomic analysis were normalized to maximum expression in each cell type across development. k-means clustering was performed using kmeans function in R (centers=10 and nstart=20).

Analysis of gene group traits

IgSF enrichment

A list of IgSF members was obtained from the InterPro database (IPR036179). Enrichment within each gene group over expected by chance was then calculated using hypergeometric distribution analysis. The set of genes expressed in a cell-type across development was taken as the universal set (N). Then number of genes in a group (n) and number of IgSFs expressed in a cell-type (m) were used as the sample size and number of successes in population respectively. Enrichment was calculated based on actual overlap between n and m, and the expected overlap

between the two, defined by (n x m)/N. For enrichment of IgSF members within cell-type dependent targets of EcR, universal set was taken as all genes expressed in all lamina neurons over development. Sample size and number of successes in the population were taken as: the total number of IgSF genes expressed over development in all lamina neurons (n), and the total number of cell-type dependent targets of EcR (m) respectively. Enrichment was calculated as described above.

Gene Ontology enrichment analysis

Gene Ontology enrichment analysis for each gene group was performed using a R package TopGO (2.36.0) using GO terms obtained from FlyBase (GO-gene association file version 2.1). Weight algorithm and Fisher's exact test were used to calculate p-value. Categories that have p-value ≤ 0.01 were considered as enriched.

Effect of perturbation of EcR and Hr3

For each perturbation, expression of each gene was normalized to maximum expression in each cell type across development and genetic background. The normalized gene expression of all genes was averaged separately for each genetic background to plot average behaviors for each gene group (Extended data Fig. 11).

Differential gene expression analysis

Wilcoxon rank-sum test (fold change ≥ 2, adjusted p-value ≤ 0.05) was used to identify genes differentially expressed between timepoints, cell-types or as a consequence of EcR/ Hr3 perturbations. Dynamic TFs and IgSF genes were defined as ones with differential expression between consecutive timepoints. Cell-type dependent genes were defined as ones with differential expression in at least one pairwise comparison amongst all lamina neurons. Cell-type specific

519 genes were defined as ones that are differentially expressed in all pairwise comparison including
520 one lamina neuron-type. Bonferroni adjustment was used for multiple testing correction.

521 **Reactome pathway analysis**

522 Dynamic transcription factors (separately for each cell-type) were entered into the
523 'Analyze Data' tool on reactome.org (https://reactome.org/PathwayBrowser/#TOOL=AT).
524 Reactome pathway analysis for *Drosophila melanogaster* was then run with default parameters.

525 **TF binding site analysis**

526 i-cisTarget (https://gbiomed.kuleuven.be/apps/lcb/i-cisTarget/)[24] was used (using default
527 parameters) to identify TF binding sites enriched within putative cis-regulatory regions and
528 ATAC-Seq peaks. dm6 version of the *Drosophila* genome, and version 5 of the i-cisTarget
529 database were used for all analyses. All ATAC-Seq peaks overlapping with transcription start sites
530 were excluded from TF binding site analyses to reduce the occurrence of promoter-enriched
531 sequence motifs in i-cisTarget results.

532 All EcR-pathway TF binding motifs enriched within different sets of ATAC-Seq peaks
533 were additionally verified using the Homer (v4.7) mergePeaks utility[53]. Briefly: first, the top 5000
534 occurrences of the motif across the genome were called using the homer scanMotifGenomeWide
535 utility. Second, Homer suite mergePeaks was then used to evaluate if the extent of overlap between
536 the top 5000 occurrences of the motif and the set of ATAC-Seq peaks is higher than expected by
537 chance. p-value ≤ 0.01 was considered as significantly more overlap than expected by chance.

Immunohistochemistry and microscopy

Immunohistochemistry and microscopy were performed as described in Xu *et al.*[54] with the following modifications: 1) For experiments involving staining of lamina neuron presynaptic sites, brains were fixed using glyoxal (3.12% glyoxal, 0.75% acetic acid and 20% ethanol, pH adjusted to 5.0) for 30' at RT and then washed 3X with PBST. 2) All images were acquired using an LSM880 confocal microscope.

Primary antibodies used in this study were: mAb24B10 (1:20, DSHB), rabbit anti-NetB (1:500, gift from Akin Lab), rabbit anti-dsRed (1:400, Clontech 632496), chicken anti-GFP (1:1000, Abcam ab13970), rat anti-Flag (1:200, Novus Biologicals, NBP1-06712), mouse anti-EcR-B1 (1:20, DSHB AD4.4), mouse anti-EcR-A (1:10, DSHB 15G1a), rabbit anti-Hr3 (1:50, gift from Thummel Lab), mouse anti-svp (1:20, DSHB 5B11), rabbit anti-erm (1:100, gift from Wang Lab), rat anti-bab2 (1:500, gift from Laski Lab), mouse anti-V5 (1:200, BioRad MCA1360), guinea pig anti-Bsh (1:400, see Tan *et al.* 2015).

Secondary antibodies used in this study were: goat anti-mouse 488 (1:500, ThermoFisher A-32723), goat anti-mouse 568 (1:500, ThermoFisher A-11031), goat anti-mouse 647 (1:500, ThermoFisher A-21235), goat anti-chicken 488 (1:1000, ThermoFisher A-11039), goat anti-rabbit 568 (1:500, ThermoFisher A-11011), goat anti-guinea pig 647 (1:500, ThermoFisher A-21450), goat anti-rabbit 647 (1:200, ThermoFisher A-32733), goat anti-rat 568 (1:500, ThermoFisher A-11077).

Image analysis

All images for figures were created using ImageJ (v2.1.0). Details for quantification of phenotypes are given below.

R8 targeting

Imaris (v9.1.2) was used to measure the distance of R8 terminals from the top of the medulla (M0), as well as the distance of 6th medulla layer (M6) from the top of the medulla. The latter was estimated using mAb24B10 staining, which labels R7 neurons that terminate in M6. Values reported on the X-axis of Fig. 3c are (R8-M0)/ (M6-M0).

L5 morphological defects

Imaris was used to visualize individual neurons. Each neuron was then manually assigned to one of the stated categories.

Quantification of BRP puncta in the lamina

The distance between the proximal end of the lamina and the distal end of the lamina was measured using Imaris individually for all lamina cartridges. A line was drawn at the measured distance divided by 2. All BRP puncta more distal of this line were counted manually.

Ex vivo culture of dissected brains

We used a protocol similar to the one described in Özel *et al.*[28] Briefly, brains were dissected from 22hAPF pupae in pre-warmed medium (ThermoFisher #2172004) with either 1:1000 dilution of 1mg/ml 20-HydroxyEcdysone (dissolved in 100% Ethanol, Sigma H5142) or equivalent volume of 100% ethanol. Brains were then incubated in ~ 200ul of medium ± 20-HydroxyEcdysone in 96 well plates for 26h at 25ºC in a humidified chamber. Thereafter, brains were fixed, stained and imaged using the aforementioned protocols for immunohistochemistry and microscopy.

In the presence of 20-HydroxyEcdysone in the media, strong expression of EcR-B1 and Hr3 is observed throughout the optic lobe, while no expression of Ftz-f1 is seen (Extended data

Fig. 13a). When 20-HydroxyEcdysone is omitted from the culture medium, no expression of Hr3 is seen (as expected), however weak induction of Ftz-f1 is observed. *In vivo,* by 22hAPF (when brains are removed from pupae), Ecdysone levels have begun to rise and may be sufficient to activate EcR-B1 in neurons[21]. As Hr3 activation requires a subsequent drop in Ecdysone titers[17], we expect the weak expression of Ftz-f1 may be due to the transfer of 22hAPF brains to an Ecdysone-free medium.

Other statistics

To compare the dynamics of genes affected by EcR^{DN} (fold change ≥ 2, p-value ≤ 0.05 between WT and EcR^{DN} at any time point) and genes unaffected by EcR^{DN}, normalized wildtype expression for each gene was divided by the maximum expression at any time point throughout development. Variance was then calculated for each gene over time. Two-tailed Student's t-test was then used to calculate the statistical difference between the distributions of variance for these two sets of genes. This was done separately for each cell-type.

Hypergeometric test was used to evaluate enrichment of targets of Erm within L3-specific targets of EcR. The set of genes expressed in a L3 neurons across development was taken as the universal set (N). Then number of targets of Erm from Peng *et al.*[32] (m) and number of L3-specific targets of EcR (n) were used as the number of successes in population and sample size respectively.

For all box-plots, solid line depicts median, while the upper and lower bounds of the box depict the third and first quantile of the data spread respectively.

Kolmogorov-Smirnov (KS) test (Fig. 3c, 16c), two-tailed Student's t-test (Extended data Fig. 7e, 7f, 11, 15a), two-tailed Fisher's exact test (Fig. 3e, 4a) were performed using the following

603 basic R functions (R 3.6.1) respectively: ks.test, t.test, fisher.test. Raw data for all analyses is
604 available upon request.

605 **Data and code availability**

606 All raw sequencing data and codes will be provided upon request. They will be made
607 publicly available prior to publication.

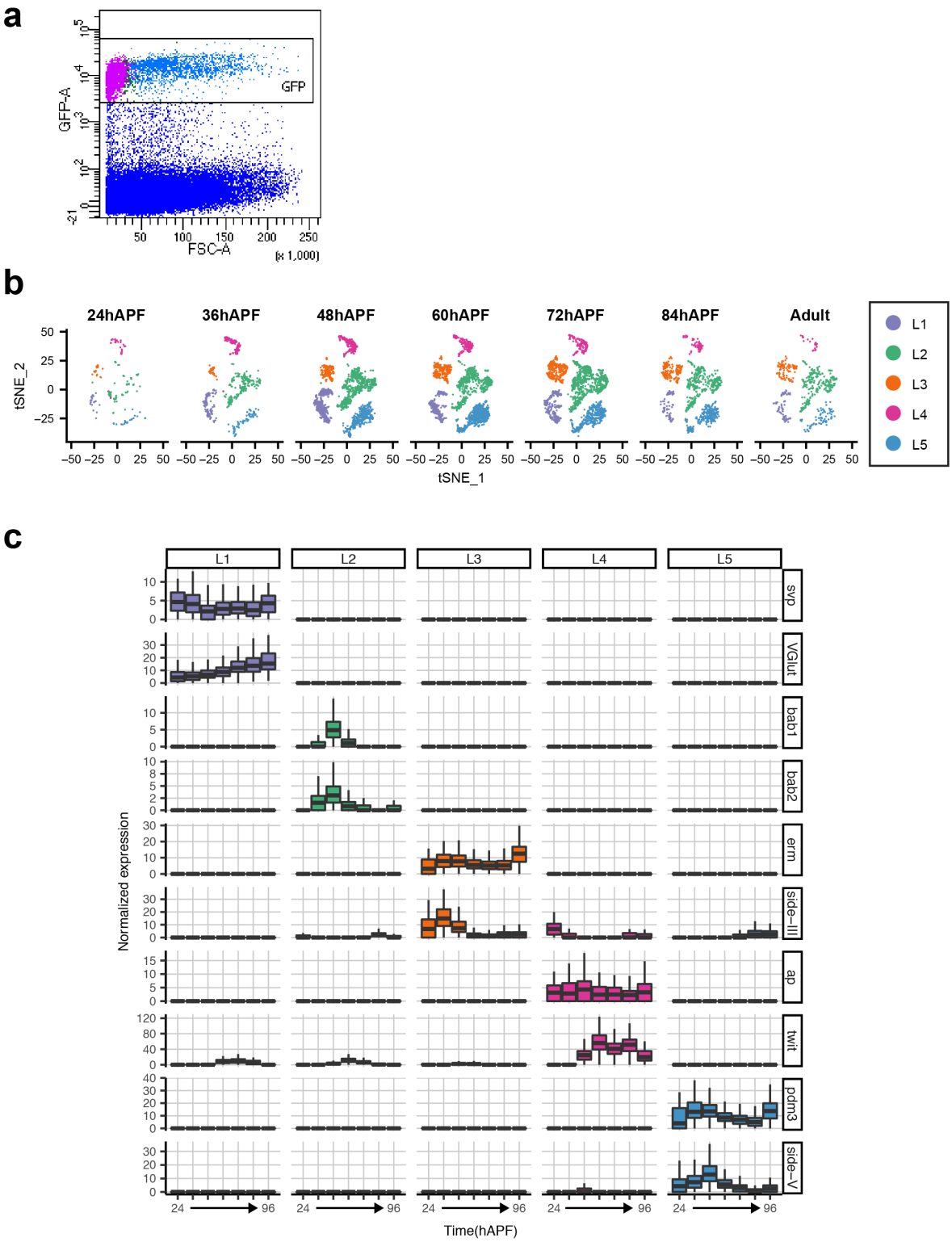

608 **Extended data Fig. 1 | scRNA-Seq-based transcriptomic analysis of lamina neurons across**

609 **development. a,** GFP vs forward scatter 2-D plot showing criteria used to enrich for lamina

610 neurons by FACS. 'Cells' highlighted in purple were excluded despite being GFP+ due to their
611 small size. **b,** tSNE plots showing L1-L5 clusters at 24hAPF, 36hAPF, 48hAPF, 60hAPF, 72hAPF,
612 84hAPF and 96hAPF (Adult). **c,** Normalized expression of previously identified lamina neuron-
613 type-specific genes in L1-L5 clusters identified at each time point over development (see Tan *et*
614 *al.*[12]).

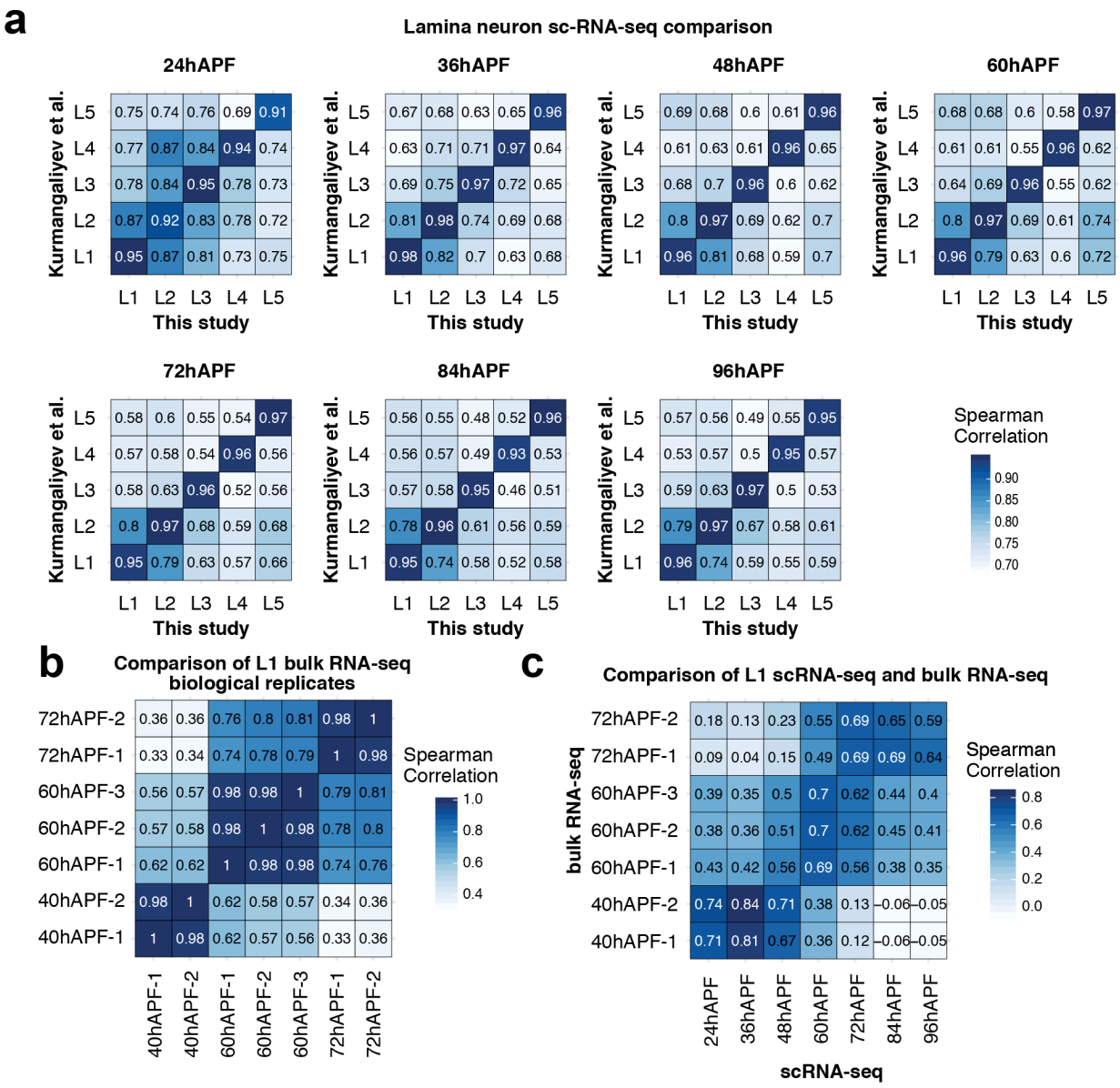

615 **Extended data Fig. 2 | Comparison of scRNA-Seq-derived transcriptome with other datasets.**

616 **a,** Comparison of lamina neuron transcriptomes generated by scRNA-Seq in this study and by

617 scRNA-Seq in Kurmangaliyev *et al*. **b,** Comparison of replicates of bulk-RNA-Seq of L1 neurons

618 at 40hAPF, 60hAPF and 72hAPF (this study). **c,** Comparison of lamina neuron transcriptomes

619 generated by scRNA-Seq in this study and by bulk RNA-Seq, also this study. See Methods for

620 calculation of Spearman correlation.

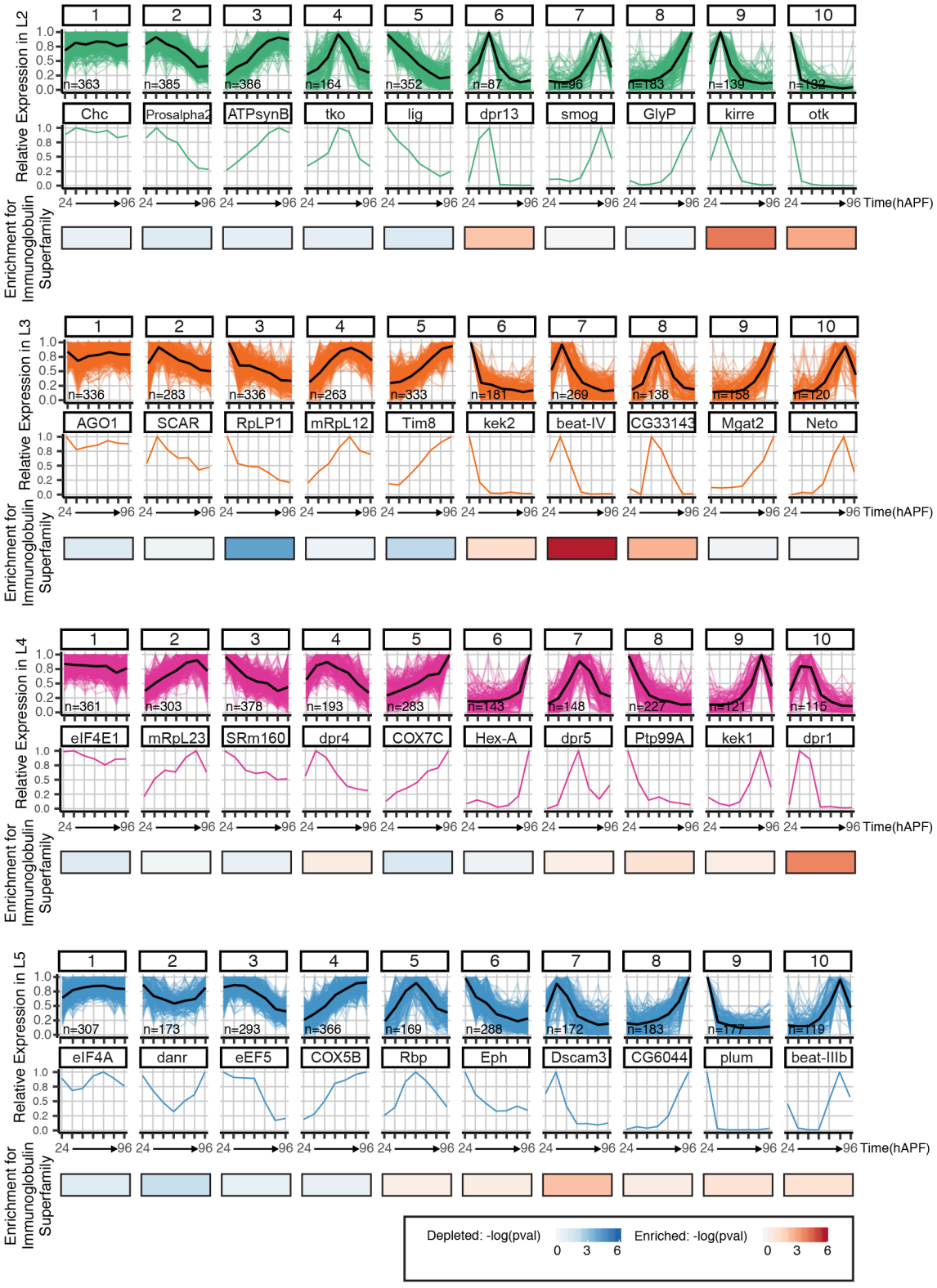

Extended data Fig. 3 | Gene groups generated via k-means clustering. Gene groups generated via k-means clustering using expression dynamics in L2-L5 neurons (see Methods). Relative

623 expression over development for each gene in the group is shown as a line plot (colored lines),
624 with the mean shown as a black line. n, number of genes in the group. A gene from each group is
625 shown. Heat map depicts enrichment ($-\log_{10}$ p-values) of Immunoglobulin Superfamily genes over
626 that expected by chance (see Methods).

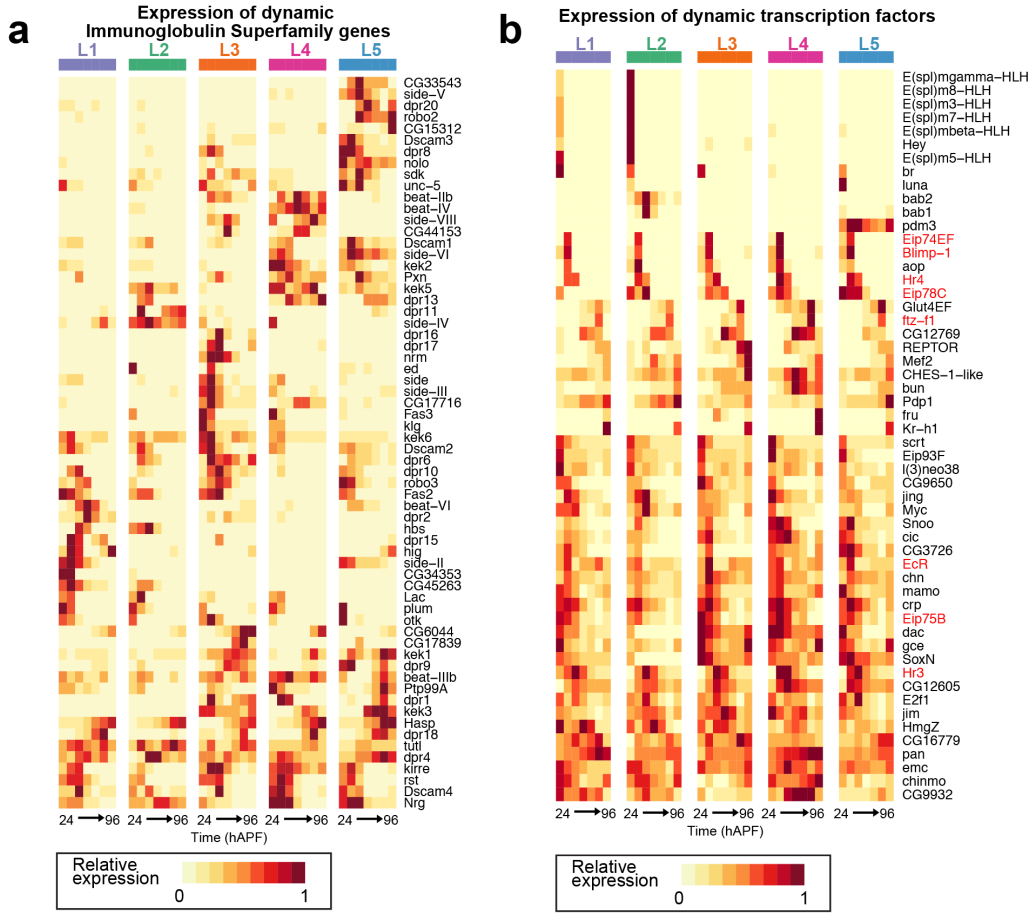

c Reactome Pathway Enrichment Analysis

Reactome Pathway in L1	p-value
Nuclear Receptor transcription pathway	$7.5X10^{-6}$
SUMOylation of intracellular receptors	$1.1X10^{-4}$

Reactome Pathway in L2	p-value
Nuclear Receptor transcription pathway	$7.4X10^{-8}$
SUMOylation of intracellular receptors	$1.7X10^{-7}$

Reactome Pathway in L3	p-value
Nuclear Receptor transcription pathway	$1.3X10^{-7}$
SUMOylation of intracellular receptors	$7.4X10^{-7}$
SUMO E3 ligases SUMOylate target proteins	$1.2X10^{-3}$
SUMOylation	$1.3X10^{-3}$
Generic Transcription Pathway	$3.6X10^{-3}$

Reactome Pathway in L4	p-value
Nuclear Receptor transcription pathway	$1.3X10^{-9}$
SUMOylation of intracellular receptors	$6.0X10^{-9}$
SUMO E3 ligases SUMOylate target proteins	$6.4X10^{-5}$
SUMOylation	$7.7X10^{-5}$
Generic Transcription Pathway	$4.4X10^{-4}$
RNA polymerase II transcription	$2.1X10^{-3}$
Gene expression (transcription)	$5.3X10^{-3}$

Reactome Pathway in L5	p-value
Nuclear Receptor transcription pathway	$9.4X10^{-7}$
SUMOylation of intracellular receptors	$1.0X10^{-5}$
Transcription of E2F targets under negative control by DREAM complex	$1.0X10^{-4}$
G0 and Early G1	$3.5X10^{-4}$
Binding of TCF/LEF:CTNNB1 to target gene promoters	$6.0X10^{-4}$
RUNX3 regulates WNT signaling	$6.0X10^{-4}$
Repression of WNT target genes	$1.5X10^{-3}$
Transcriptional regulation of granulopoeisis	$2.1X10^{-3}$
Transcription of E2F targets under negative control by p107 (RBL1) and p130 (RBL2) in complex with HDAC1	$2.2X10^{-3}$
TP53 Regulates Transcription of Genes Involved in G1 Cell Cycle Arres	$2.4X10^{-3}$
SUMO E3 ligases SUMOylate target proteins	$5.4X10^{-3}$
SUMOylation	$6.2X10^{-3}$
Generic Transcription Pathway	$7.8X10^{-3}$
SMAD2/SMAD3:SMAD4 heterotrimer regulates transcription	$8.6X10^{-3}$

Extended data Fig. 4 | IgSF coding genes and some TFs show dynamic expression over development. a, Heat map showing relative expression of genes encoding Immunoglobulin

629 Superfamily proteins with dynamic expression in at least one lamina neuron-type over
630 development (64 genes, ≥ 2-fold change in expression between any consecutive time points, p-
631 value <0.05). Each row represents a different gene. Each column is a different time-point every
632 12h from 24 to 96 hAPF (Adult). Note the cell-type dependent patterns of expression of IgSF
633 coding genes. **b,** Heat map showing relative expression of dynamic transcription factors (see
634 Methods). Many members of the Ecdysone signaling pathway are highlighted in red. **c,** Reactome
635 pathway analysis of dynamic TFs showing all enriched categories (p-value < 0.01). Enrichment of
636 the Nuclear Receptor Transcription Pathway is highlighted in L1-L5 neurons.

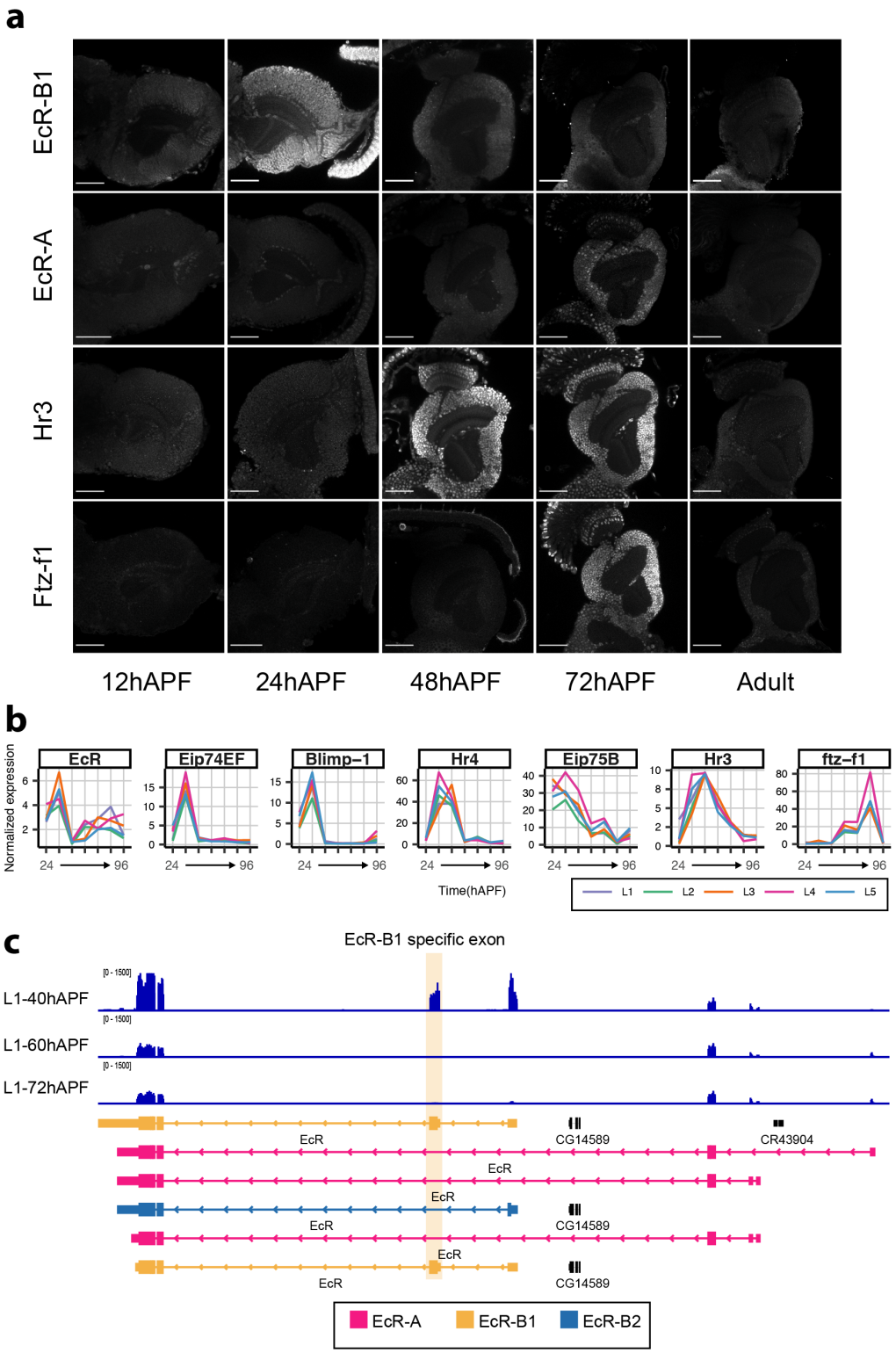

637 **Extended data Fig. 5 | Expression of TFs in the Ecdysone cascade. a,** Images showing immuno-

638 staining for EcR-B1, EcR-A, Hr3 and Ftz-f1 at 12hAPF, 24hAPF, 48hAPF, 72hAPF and in adults.

639 Note that an anti-GFP antibody was used to stain for Ftz-f1 in fly lines carrying a BAC with GFP-
640 tagged Ftz-f1 and endogenous cis-regulatory sites (see Supplementary Table 1). Scale bar, 50μm.
641 **b**, Line plots of expression of TFs. **c,** Read pile-up in the EcR locus showing change of isoform
642 from predominantly EcR-B1 to EcR-A between 40hAPF and 60hAPF.

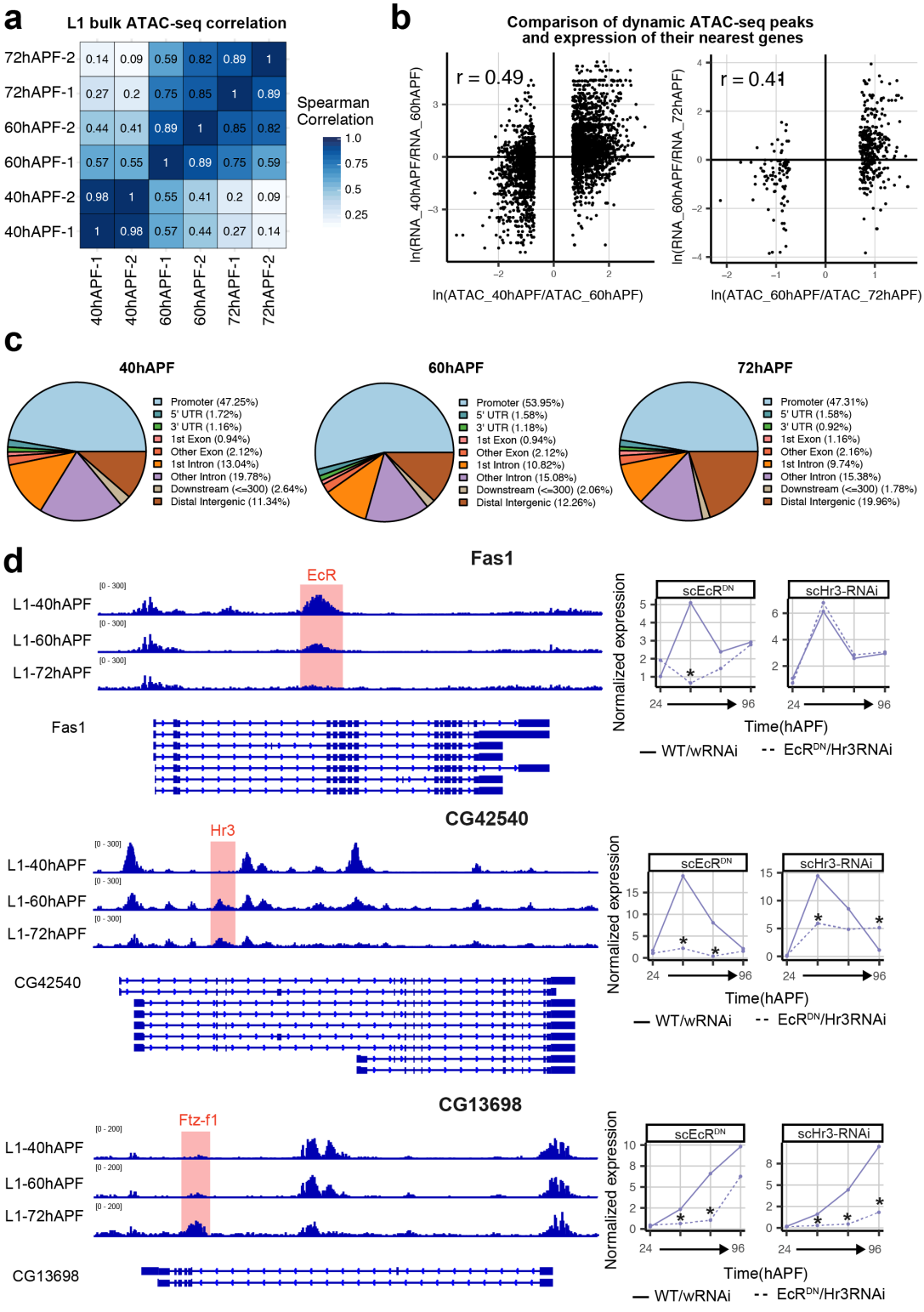

643 **Extended data Fig. 6 | ATAC-Seq analysis of developing L1 neurons. a,** Comparison of

644 replicates of bulk ATAC-Seq data of L1 neurons at 40hAPF, 60hAPF and 72hAPF. Values shown

645 are Spearman correlation values (see Methods). **b**, Comparison of change of ATAC-seq peak
646 coverage and change in expression of nearest gene. ln(fold change RPKM of nearest gene) vs
647 ln(fold change ATAC-seq peak coverage) between 40hAPF and 60hAPF, and 60hAPF and
648 72hAPF. r, Pearson's correlation coefficient. **c,** Distribution of the top 5000 peaks at each time
649 point between various genomic landmarks. **d,** Normalized ATAC-Seq read pile-ups are shown for
650 L1 neurons at 40hAPF, 60hAPF and 72hAPF for three gene loci – Fas1, CG42450, CG13698.
651 ATAC-Seq peaks with predicted binding sites for EcR, Hr3 and Ftz-f1 are highlighted. Shown
652 along with is normalized expression of these genes in control (solid line) vs EcR^{DN} or Hr3 RNAi
653 expressing L1 neurons (dashed lines).

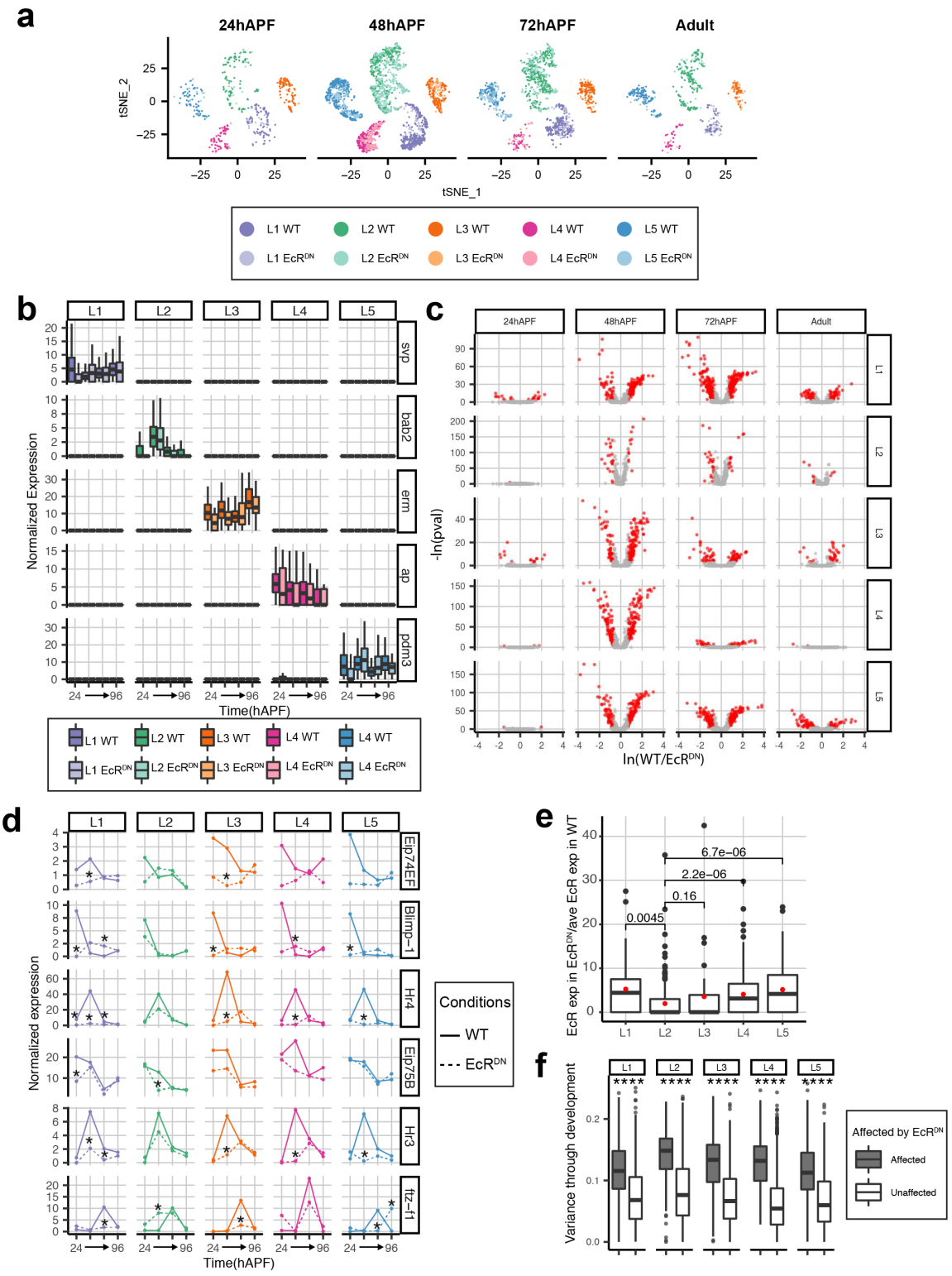

654 **Extended data Fig. 7 | scRNA-Seq-based analysis of WT and EcR^{DN} expressing lamina**

655 **neurons. a,** tSNE plots showing WT and EcR^{DN}-expressing L1-L5 clusters at 24hAPF, 48hAPF,

72hAPF, and 96hAPF (Adult). **b,** Expression of lamina neuron-type-specific TFs ± EcR^{DN} expression. **c,** Volcano plots showing significant gene expression changes in L1-L5 neurons throughout development. Red dots: fold change ≥ 2 and p-value ≤ 0.05. **d,** Normalized expression of TFs in the Ecdysone-signaling pathway in WT (solid lines) and EcR^{DN}-expressing (dashed lines) L1-L5 neurons. *, p-value ≤ 0.05, fold change ≥ 2. **e.** Expression of EcR in EcR^{DN}-expressing lamina neurons at 48hAPF normalized to mean expression of EcR in wildtype cells at 48hAPF (done separately for each lamina neuron-type). Red dots, mean of data spread. Increase in EcR expression in EcR^{DN}-expressing cells over wildtype is expected to be due to the expression of the EcR^{DN} transgene. Note the poor induction of EcR^{DN} in L2 neurons. p-value from student's t-test are stated in the figure for comparison between L2 and other lamina neuron-types. The difference between EcR^{DN} expression in L2 and L3 neurons is not significant likely due to the low cell numbers of EcR^{DN}-expressing L3 neurons. **f,** Comparison of variance of wildtype expression of genes affected or unaffected by EcR^{DN} expression (see methods). ****, p-value < 0.0001, student's t-test.

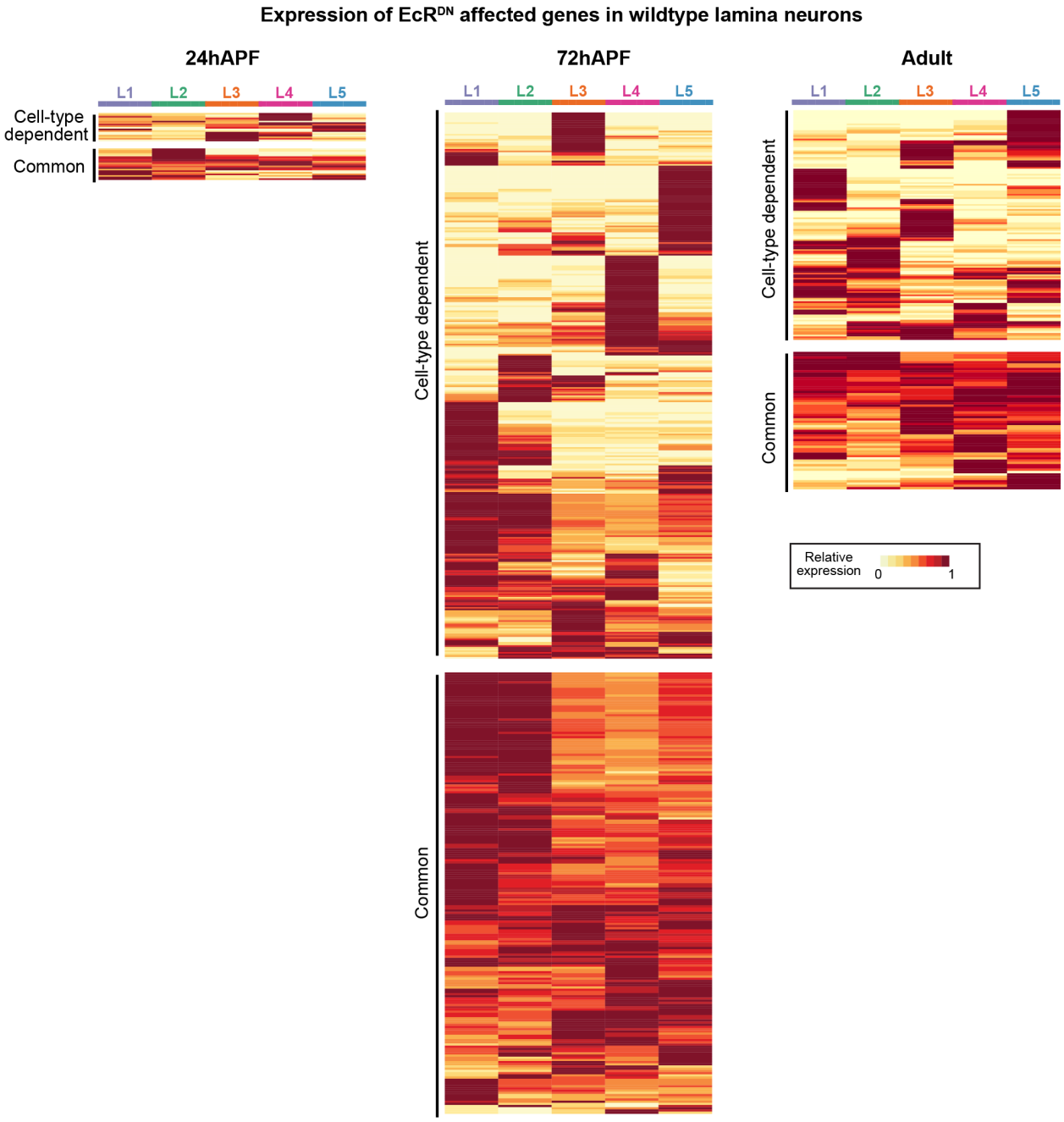

670 **Extended data Fig. 8 | Cell-type dependent targets of EcR.** Heat map showing relative
671 expression in wildtype cells of genes affected by EcR^{DN} at 24hAPF, 72hAPF and in adults. Targets
672 of EcR are divided into two categories: Cell-type dependent (in any pairwise comparison fold
673 change ≥ 2, p-value ≤ 0.05) and Common targets (no significant expression difference in any
674 pairwise comparison) (see Fig. 2c and Methods).

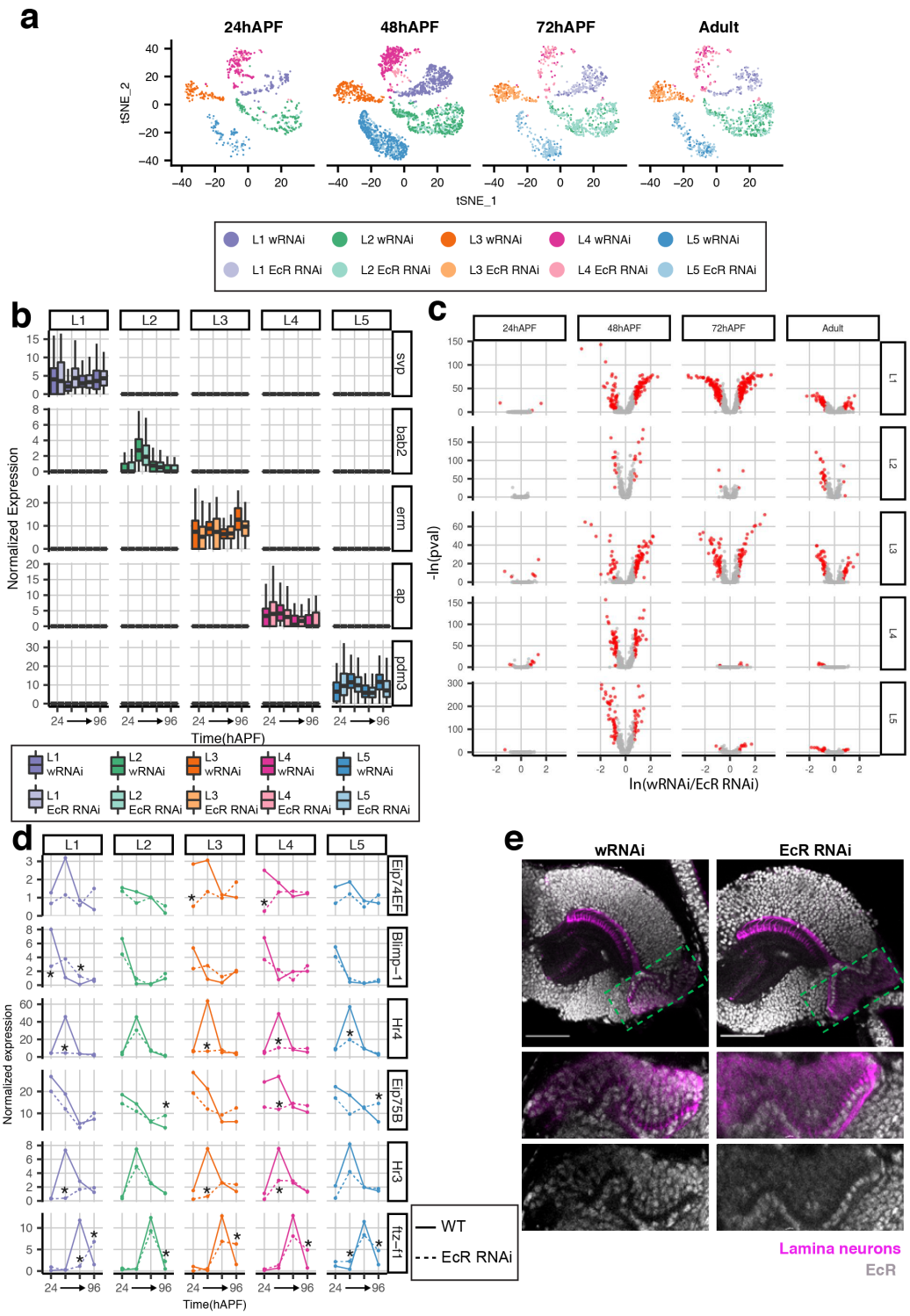

675 **Extended data Fig. 9 | scRNA-Seq-based analysis of wRNAi (control) and EcR RNAi**

676 **expressing lamina neurons. a,** tSNE plots showing wRNAi and EcR RNAi-expressing L1-L5

clusters at 24hAPF, 48hAPF, 72hAPF, and 96hAPF (Adult). **b,** Expression of lamina neuron-type-specific TFs ± EcR RNAi expression. **c,** Volcano plots showing significant gene expression changes in L1-L5 neurons throughout development. Red dots: fold change ≥ 2 and p-value ≤ 0.05. **d,** Average expression of TFs in the Ecdysone-signaling pathway in wRNAi (solid lines) and EcR RNAi-expressing (dashed lines) L1-L5 neurons. *, p-value ≤ 0.05, fold change ≥ 2. **e,** Image showing optic lobe (top) stained using an antibody targeting all EcR isoforms (grey) at 24hAPF. Box with green dotted outline marks the region containing lamina neuron cell-bodies. This region is magnified in bottom two panels. Lamina neurons are labeled in magenta. Scale bar, 50μm.

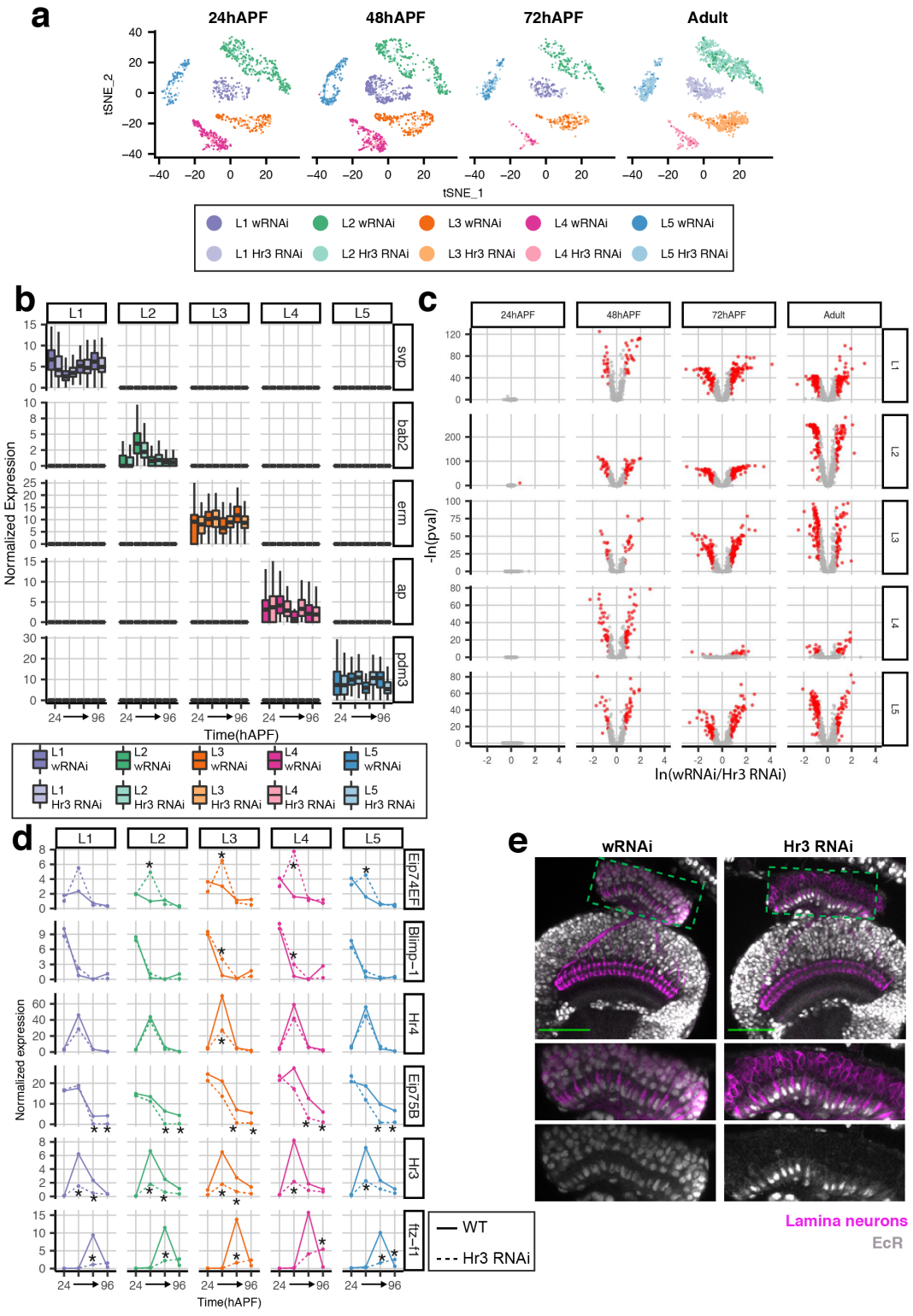

685 **Extended data Fig. 10 | scRNA-Seq-based analysis of wRNAi (control) and Hr3 RNAi**

686 **expressing lamina neurons. a,** tSNE plots showing wRNAi and Hr3 RNAi-expressing L1-L5

clusters at 24hAPF, 48hAPF, 72hAPF, and 96hAPF (Adult). **b,** Expression of lamina neuron-type-specific TFs ± Hr3 RNAi expression. **c,** Volcano plots showing significant gene expression changes in L1-L5 neurons throughout development. Red dots: fold change ≥ 2 and p-value ≤ 0.05. **d,** Average expression of TFs in the Ecdysone-signaling pathway in wRNAi (solid lines) and Hr3 RNAi-expressing (dashed lines) L1-L5 neurons. *, p-value ≤ 0.05, fold change ≥ 2. **e,** Image showing optic lobe (top) stained using an antibody targeting Hr3 (grey) at 48hAPF. Box with green dotted outline marks the region containing lamina neuron cell-bodies. This region is magnified in bottom two panels. Lamina neurons are labeled in magenta. Scale bar, 50μm. Also see panel d for efficiency of Hr3 knockdown.

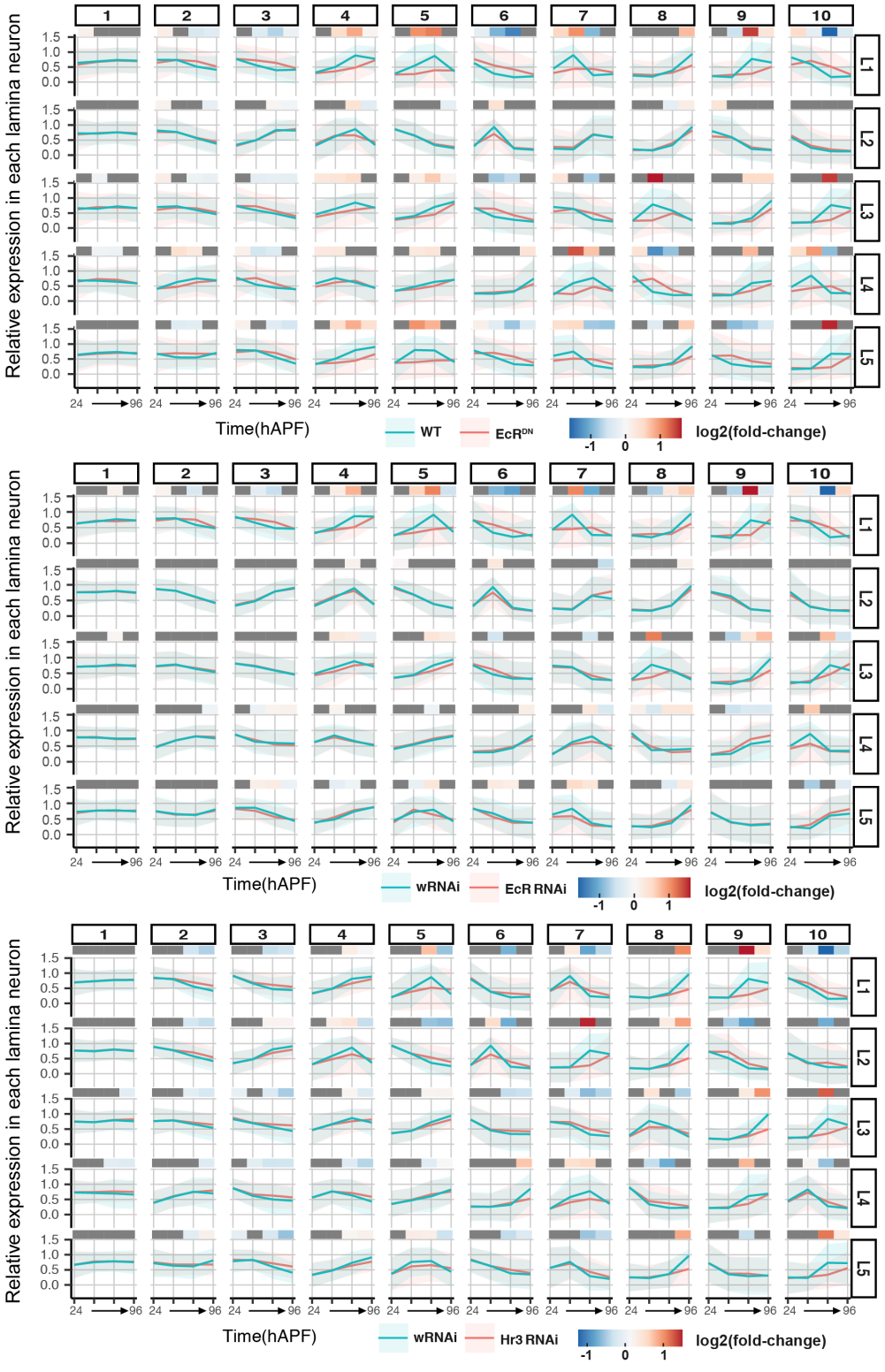

696 **Extended data Fig. 11 | Effect of EcR^{DN}, EcR RNAi and Hr3 RNAi on k-means cluster**

697 **generated gene groups.** Relative expression of genes in control (aqua) or perturbation of EcR or

698 Hr3 activity (orange) for each gene group in L1-L5 neurons generated via k-means clustering (see
699 Fig. 1c, Extended data Fig. 3). Average behavior of genes in a group for control and perturbation
700 of EcR or Hr3 activity are shown in bold lines, while standard deviation is shown in shaded region
701 of the same color. Heat map shows Log_2 (Fold change) between average of WT and average of
702 perturbation for all comparisons where student's t-test p-value < 0.01.

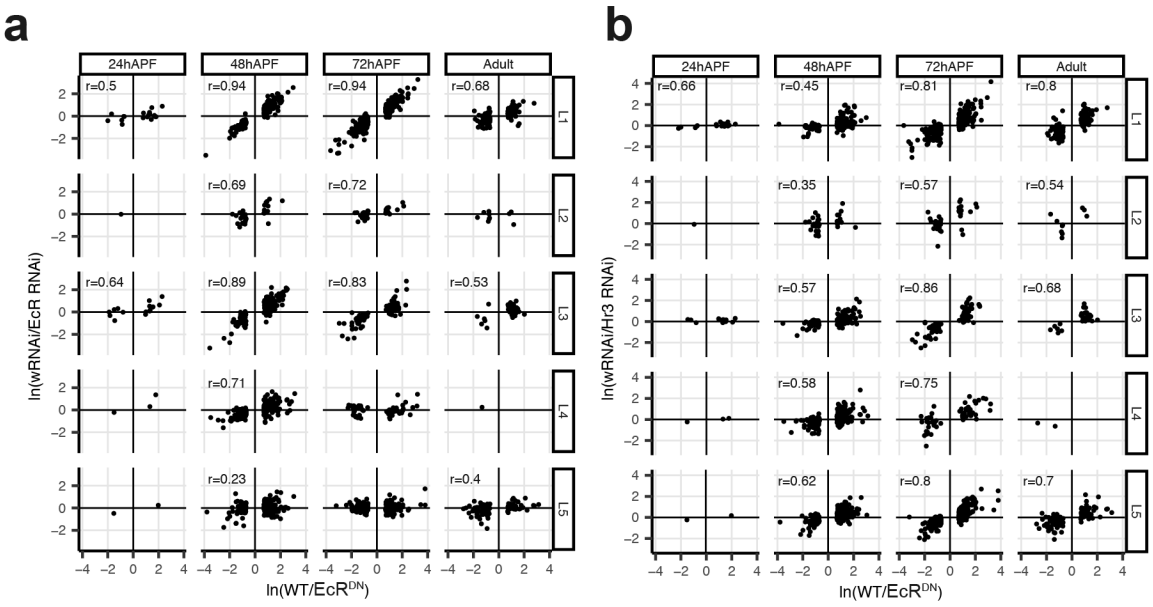

703 **Extended data Fig. 12 | Comparison of transcriptomic changes in EcR^{DN}, EcR RNAi and Hr3**
704 **RNAi. a,** ln(normalized expression in wRNAi/EcR RNAi) vs ln(normalized expression in
705 WT/EcR^{DN}) for L1-L5 neurons throughout development. **b,** ln(normalized expression in
706 wRNAi/Hr3 RNAi) vs ln(normalized expression in WT/EcR^{DN}) for L1-L5 neurons throughout
707 development. **a, b,** r, Pearson's correlation coefficient.

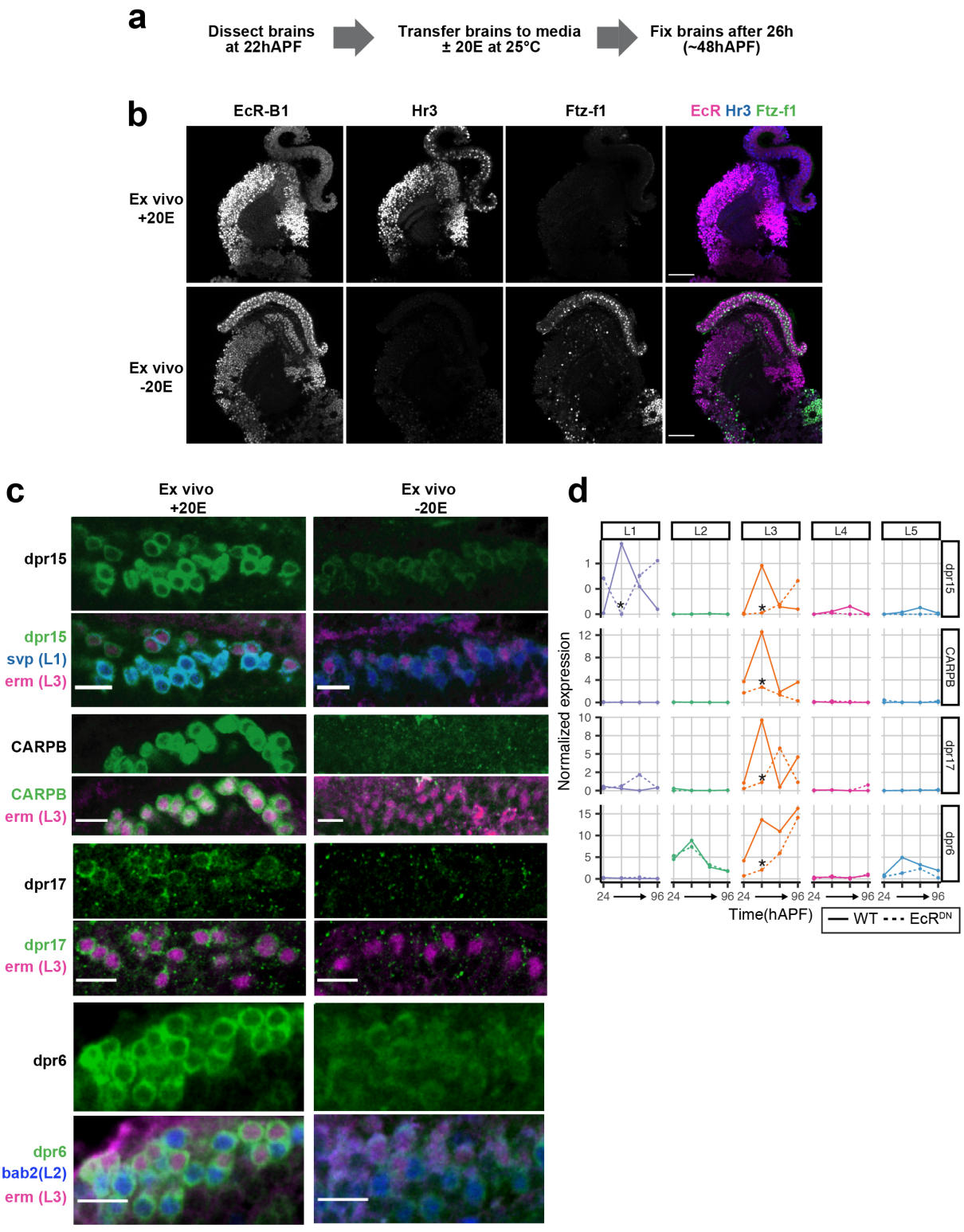

708 **Extended data Fig. 13 | Gene expression in *ex vivo* brain cultures with and without Ecdysone.**

709 **a,** Design for *ex vivo* brain culture with or without 20-HydroxyEcdysone (20E). **b,** Expression of

710 EcR-B1, Hr3 and Ftz-f1 in brain explants ± inclusion of 20E in the culture medium. Scale bar,
711 50µm. See Methods. **c,** Staining for protein-traps or GFP-Mimic reporter lines for dpr15, CARPB,
712 dpr17 and dpr6 (genes with cell-type-dependent patterns of expression and predicted to require
713 Ecdysone for expression from our sequencing data) ± inclusion of 20E in the medium. Scale bar,
714 10µm. Different lamina neurons are labeled using antibodies against lamina neuron-type-specific
715 TFs (see Extended data Fig. 1c). **d,** Normalized expression of dpr15, CARPB, dpr17 and dpr6 in
716 wildtype (solid lines) and EcR^{DN}-expressing (dashed lines) L1-L5 neurons throughout
717 development. *, p-value ≤ 0.05, fold change ≥ 2. Note that dpr6 shows Ecdysone-dependent
718 expression in L2 neurons in *ex vivo* cultured brains, but seems to be unaffected by EcR^{DN}
719 expression based on our sequencing data. This is consistent with low induction of EcR^{DN} in L2
720 neurons using the pan-lamina Gal4 driver (see Extended data Fig. 7e).

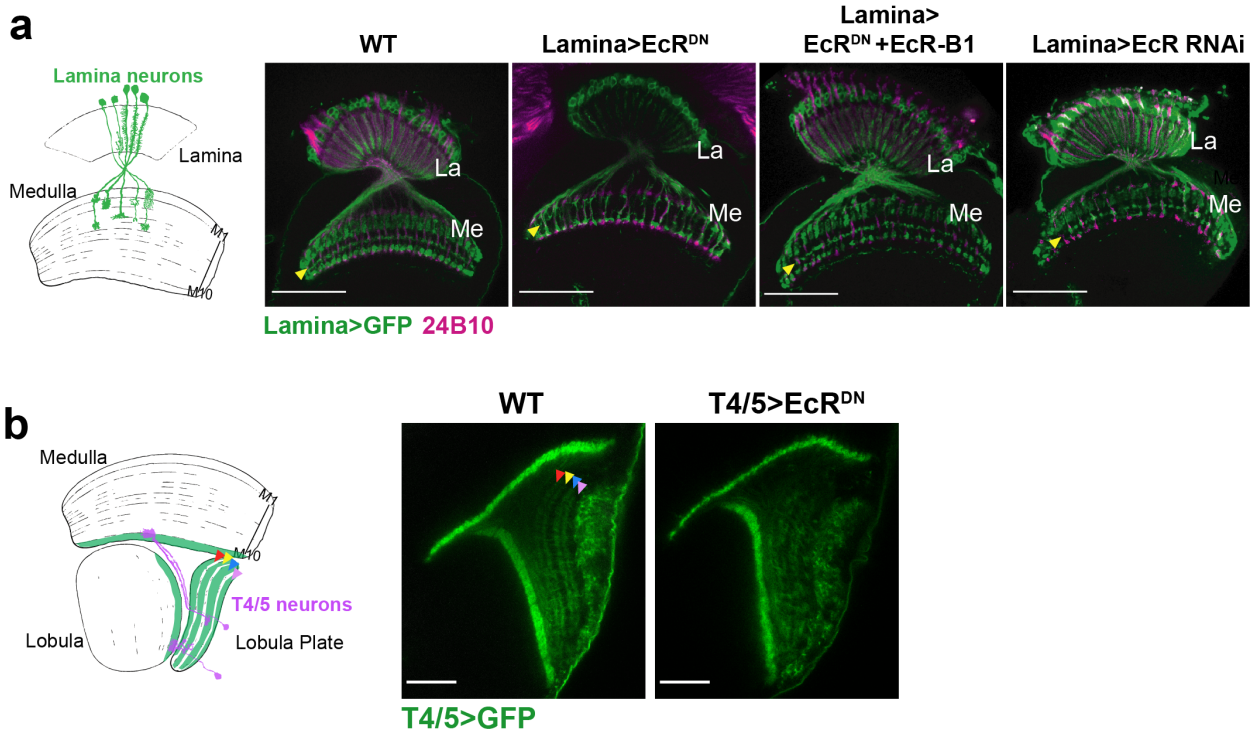

721 **Extended data Fig. 14 | Effect of EcR^{DN} on neuronal morphology. a,** Morphology of lamina
722 neurons (L1-L5) in wildtype (WT) brains and upon pan-lamina expression of EcR^{DN}, EcR^{DN} +
723 EcR-B1 cDNA and EcR RNAi. mAb24B10 labels M3 and M6. M3 is highlighted with yellow
724 arrowhead. Scale bar, 50μm. La, lamina neuropil. Me, medulla neuropil. **b,** Effect of EcR^{DN}
725 expression on morphology of T4/T5 neurons. Four layers in the lobula plate, a, b, c and d, are
726 marked with red, yellow, blue and pink arrowheads, respectively. Cartoons of one T4 (purple
727 neuron, top) and one T5 neuron (purple neuron, bottom) are shown to highlight wildtype
728 morphology. Scale bar, 20μm.

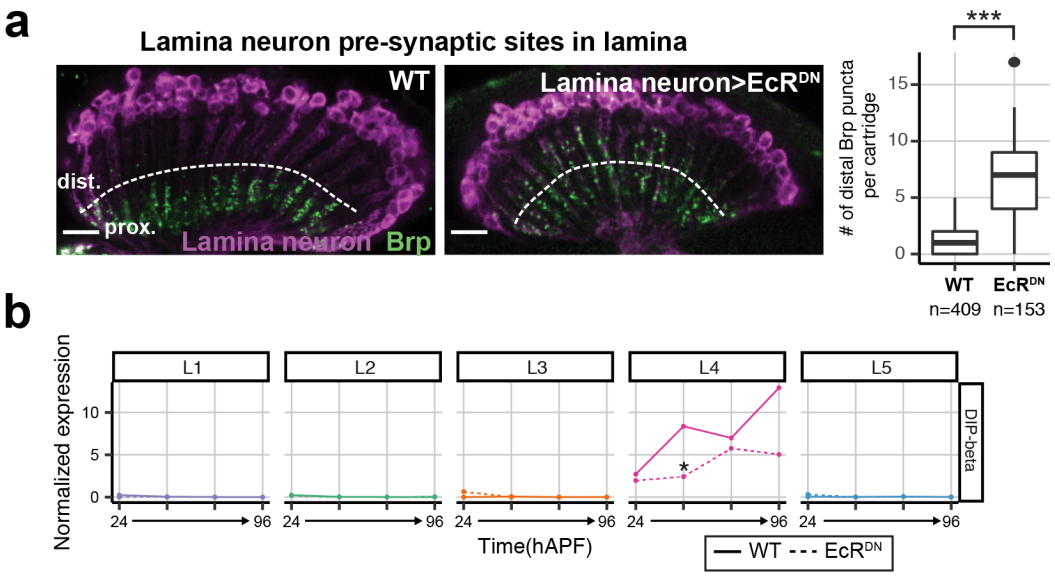

729 **Extended data Fig. 15 | Distribution of presynaptic sites in the lamina ± EcR^{DN} expression.**

730 **a,** Distribution of Brp puncta (presynaptic sites) in the lamina neuropil for wildtype (WT) and

731 EcR^{DN}-expressing lamina neurons. Magenta, all lamina neurons, Green, Brp puncta. Dotted line

732 differentiates proximal and distal halves of the lamina neuropil (see Methods). Scale bars, 50µm.

733 Distribution of distal BRP puncta/ cartridge for both conditions is also shown. ***, student's t test

734 p-value < 0.001. n, number of cartridges quantified (7 animals for wildtype, 6 animals for EcR^{DN}).

735 **b,** Normalized expression of DIP-β in wildtype (solid lines) and EcR^{DN}-expressing L1-L5 neurons

736 (dashed lines). *, p-value ≤ 0.05, fold change ≥ 2.

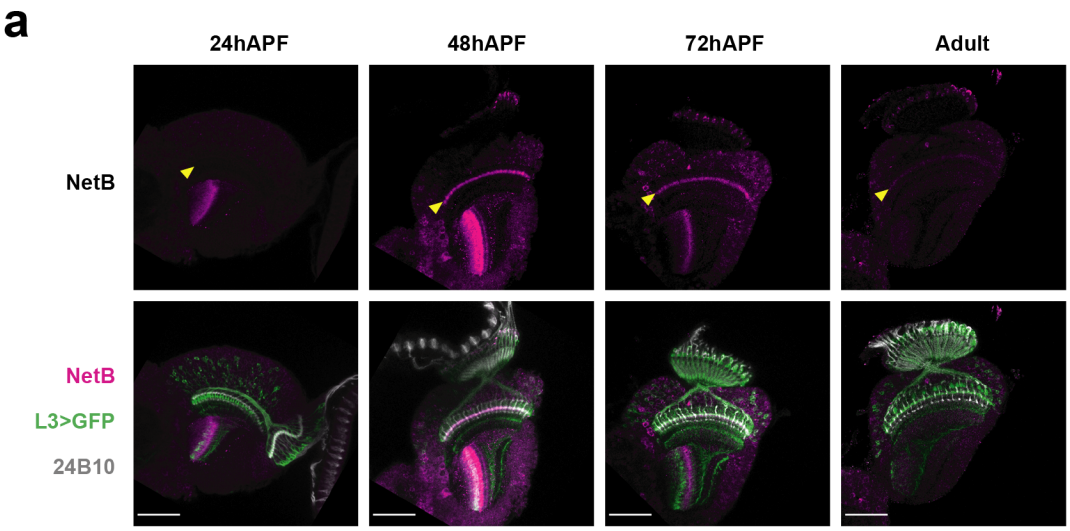

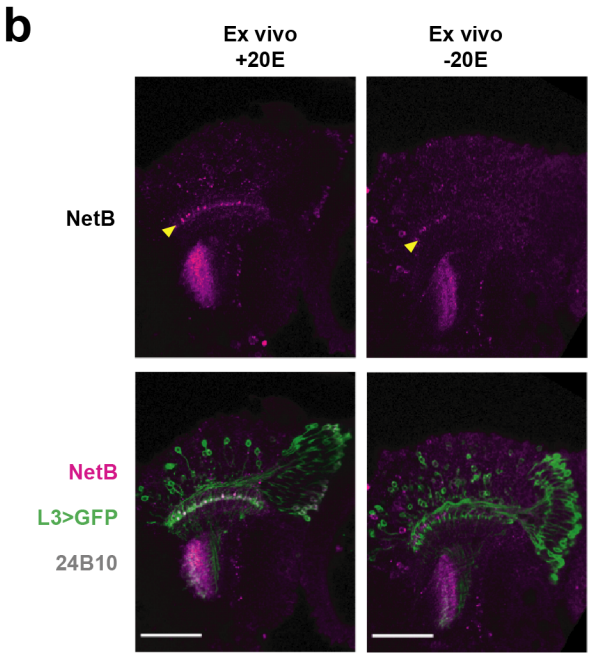

c

P-value of KS test for R8 phenotype distribution

	WT	L3> EcR^{DN}	L3> NetB	L3> EcR^{DN}+ NetB
WT	1	$<10^{-15}$	0.65	$2.2X10^{-15}$
L3> EcR^{DN}	$<10^{-15}$	1	$<10^{-15}$	$<10^{-15}$
L3> NetB	0.65	$<10^{-15}$	1	$<10^{-15}$
L3> EcR^{DN}+ NetB	$2.2X10^{-15}$	$<10^{-15}$	$<10^{-15}$	1

Extended data Fig. 16 | NetB expression dynamics and dependence on Ecdysone for expression. a, Staining for NetB (magenta) in the optic lobe at 24hAPF, 48hAPF, 72hAPF and in Adult. M3 is highlighted with a yellow arrowhead. mAb24B10 is used as a layer marker in the medulla. Note that maximum expression in M3 is seen at 48hAPF. **b,** Anti-NetB antibody staining (magenta) in *ex vivo* cultured brains ± inclusion of 20E in the medium (see Methods and Extended data Fig. 13a). In **a** and **b,** L3 neurons are labeled using myr-GFP. Scale bar, 50μm. **c,** Table

743 showing p-values from KS test for comparison of R8 axon depth distributions between all genetic

744 conditions in Fig. 3c. Note that p-value = $2.2X10^{-15}$ for comparison between L3>EcR^{DN} + NetB

745 and WT is indicative of an incomplete rescue of EcR^{DN} phenotype by NetB overexpression.

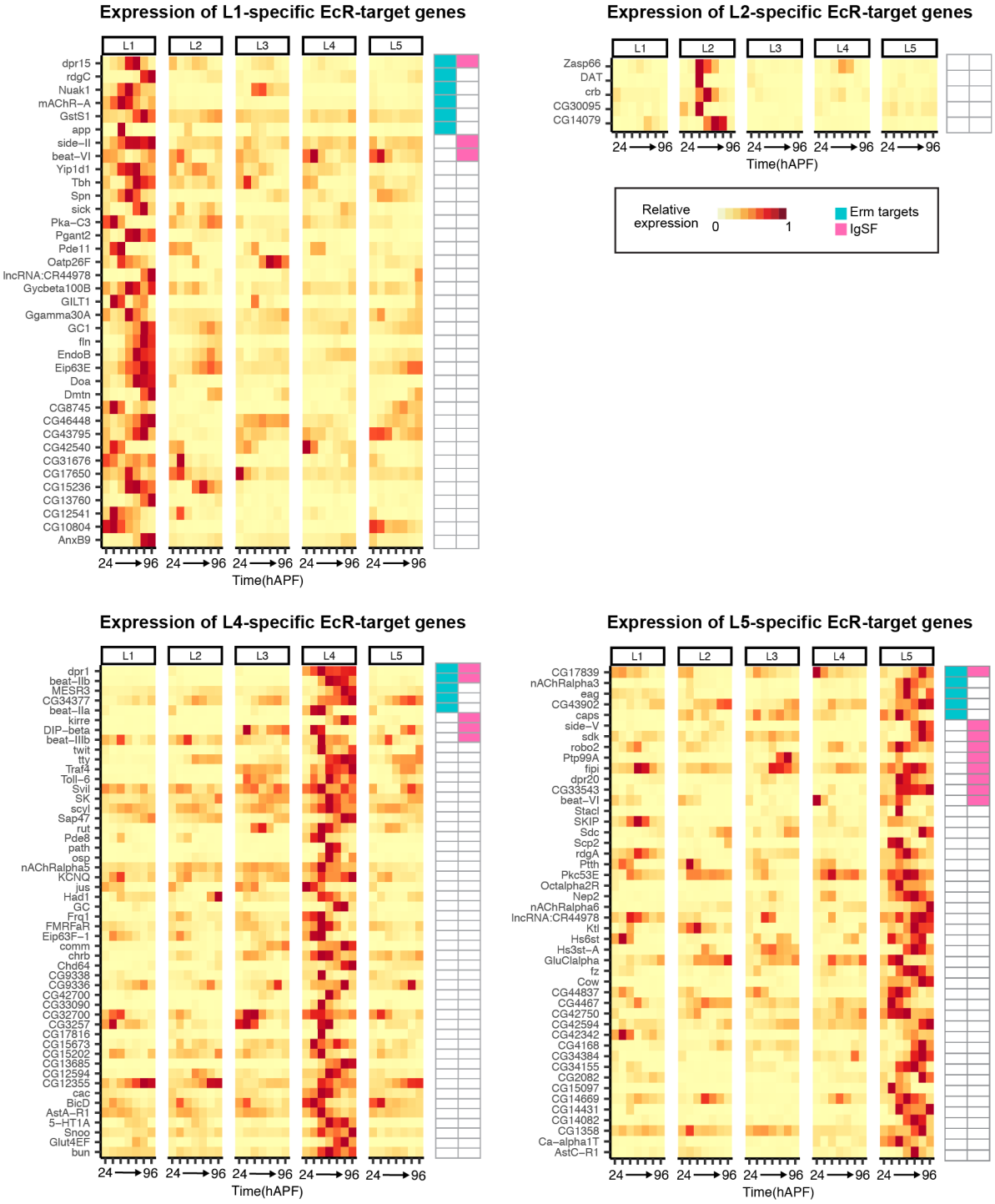

746 **Extended data Fig. 17 | L1, L2, L4 and L5 – specific targets of EcR.** Heat map showing relative
747 expression of L1, L2, L4 and L5-specific targets of EcR (see Methods). Aqua, targets of
748 transcription factor Erm identified in Peng *et al.*[32]. Magenta, Immunoglobulin Superfamily genes.

749 The relatively small number of L2-specific targets of EcR is likely to reflect low expression of

750 EcR^{DN} in these neurons (Extended data Fig. 7e).

751 **Supplementary Tables**

752 **Supplementary Table 1.** Fly strains used in this study

753 **Supplementary Table 2.** Developmental transcriptome of lamina neurons. Normalized
754 expression values are given for all expressed genes.

755 **Supplementary Table 3.** Transcriptome of L1 neurons at 40hAPF, 60hAPF and 72hAPF by bulk
756 RNA-Seq. Numbers in the table are RPKM values.

757 **Supplementary Table 4.** Gene groups generated by k-means clustering. Relative expression
758 values are given for all expressed genes.

759 **Supplementary Table 5.** Gene Ontology (GO) analysis of gene groups generated by k-means
760 clustering.

761 **Supplementary Table 6.** TF binding site analysis using i-cisTarget (see Methods).

762 **Supplementary Table 7.** ATAC-Seq analysis of L1 neurons at 40hAPF, 60hAPF and 72hAPF.
763 Measure of reads mapped to each peak are given as RPKM values. Peaks with differential
764 accessibility between consecutive time points are also given.

765 **Supplementary Table 8.** Normalized expression in WT and EcR^{DN}-expressing lamina neurons.
766 Genes differentially expressed between WT and EcR^{DN} are also given.

767 **Supplementary Table 9.** Gene Ontology (GO) analysis of common and cell-type dependent
768 targets of EcR.

769 **Supplementary Table 10.** Normalized expression in wRNAi and EcR RNAi-expressing lamina
770 neurons. Genes differentially expressed between wRNAi and EcR RNAi are also given.

771 **Supplementary Table 11.** Normalized expression in wRNAi and Hr3 RNAi-expressing lamina
772 neurons. Genes differentially expressed between wRNAi and Hr3 RNAi are also given.

773 **Supplementary Table 12.** Lists of genes likely to be involved in step 1 or step 2 of L5 axonal

774 morphogenesis (see Fig. 4c).

Acknowledgements

We thank Dr. Pecot (Harvard), Dr. Yamanaka (UC Riverside), Dr. Black (UCLA), Dr. De Robertis (UCLA), Dr. Riddiford (Univ. of Washington) and Dr. Truman (Janelia Research Campus) for helpful discussions. We thank Dr. Schuldiner (Weizmann Institute of Science) and members of the Zipursky lab for feedback on the manuscript, and Dr. Diaz de la Loza for help with figure illustrations. We would like to specifically acknowledge Juyoun Yoo's (Zipursky Lab) and Rachel Hodge's (Jones Lab, UCLA) help with ATAC-Seq library prep and immunostaining. We also thank the BSCRC Sequencing Core (UCLA) and the TCGB core (UCLA) for help with library preparation and sequencing; the BSCRC FACS core (UCLA) and the Witte lab (UCLA) for assistance with FACS purification of lamina neurons; and the IDRE Statistics Consulting (UCLA) and Dr. Balliu (UCLA) for assistance with the statistical analysis of data. Reagents provided by Dr. Akin (UCLA), Dr. Laski (UCLA), Dr. Wang (Duke-NUS), Dr. Pecot (Harvard), Dr. Thummel (Univ. of Utah) and Dr. Bashaw (Univ. of Penn.) were critical for this work. This work was supported by NIH T32-NS048004 Neurobehavioral Genetics Training Grant (S.J.), Helen Hay Whitney Foundation (S.J.) and Whitcome Fellowship (Y.L.). S.L.Z is an investigator of the Howard Hughes Medical Institute.

Author contributions

S.J., Y.L., Y.K. and S.L.Z. designed experiments. S.J., Y.L., P.M. and B.P. acquired data. S.J., Y.L. and Y.K. analyzed the data. S.J., Y.L. and S.L.Z. wrote the manuscript with input from all co-authors.

Competing interest declaration

The authors declare no competing interests.

Additional information

Supplementary Information is available for this paper.

Correspondence and requests for materials should be addressed to: Dr. S. Lawrence Zipursky - lzipursky@mednet.ucla.edu.

Additional References

50. Hoskins, R. A. *et al.* The Release 6 reference sequence of the Drosophila melanogaster genome. *Genome Res* **25**, 445–458 (2015).

51. Picelli, S. *et al.* Full-length RNA-seq from single cells using Smart-seq2. *Nat Protoc* **9**, 171–181 (2014).

52. Buenrostro, J. D., Giresi, P. G., Zaba, L. C., Chang, H. Y. & Greenleaf, W. J. Transposition of native chromatin for fast and sensitive epigenomic profiling of open chromatin, DNA-binding proteins and nucleosome position. *Nat Methods* **10**, 1213--1218 (2013).

53. Heinz, S. *et al.* Simple Combinations of Lineage-Determining Transcription Factors Prime cis-Regulatory Elements Required for Macrophage and B Cell Identities. *Mol Cell* **38**, 576–589 (2010).

54. Xu, S. *et al.* Interactions between the Ig-Superfamily Proteins DIP-α and Dpr6/10 Regulate Assembly of Neural Circuits. *Neuron* **100**, 1369--1384.e6 (2018).